Applied Mathematical Modelling 59 (2018) 183–204

Contents lists available at ScienceDirect

Applied Mathematical Modelling

journal homepage: www.elsevier.com/locate/apm

Effective elastic properties of layered composites considering non-uniform imperfect adhesion

Humberto Brito-Santana[a,*], Ricardo de Medeiros[b], Antonio Joaquim Mendes Ferreira[c], Reinaldo Rodríguez-Ramos[d], Volnei Tita[a]

[a] Department of Aeronautical Engineering, São Carlos School of Engineering, University of São Paulo, Av. João Dagnone 1100, São Carlos, SP, Brazil
[b] Santa Catarina State University, College of Technological Sciences, Mechanical Engineering Department, Composite and Vibration Group, Rua Paulo Malschitzki, 200, Joinville, SC, Brazil
[c] University of Porto, Faculty of Engineering of University of Porto, Mechanical Engineering Department, Porto, Portugal
[d] Faculty of Mathematics and Computing Sciences, University of Havana, San Lázaro esq. L, Vedado, Havana CP10400, Cuba

ARTICLE INFO

Article history:
Received 19 May 2017
Revised 4 January 2018
Accepted 10 January 2018
Available online 31 January 2018

Keywords:
Analytical model
Delamination
Finite element analysis
Interlayer
Non-uniform imperfection

ABSTRACT

In this study, the effective elastic properties of layered composites are predicted by considering the influence of non-uniform imperfect adhesion. In practical terms, the influence of non-uniform imperfection on the effective properties of layers is evaluated when debonding or delamination occurs between adjacent layers. Thus, the effective properties of two- and three-layer composites with imperfect and perfect interfaces are calculated using the finite element method and an analytical technique based on the two-scale asymptotic homogenization method, respectively. In the analyses, it was used a two-layer model with imperfect interface conditions and a three-layer model with perfect conditions to derive analytical expressions of the interlayer properties, which are equivalent to the effect of the imperfection (e.g., debonding). Our numerical results demonstrate that the three-layer model provides an excellent approximation of the two-layer one and it illustrates how the effective properties of the layered composites made from titanium Ti6Al4V and ceramic AD-96 are affected by non-uniform imperfect adhesion.

1. Introduction

Adhesively bonded joints are used in a wide range of applications in the automotive, aeronautical, and other industries. The requirements for the design of lightweight structures and the increased use of lightweight materials in industrial fields have led to the widespread use of adhesive joints in recent years. Applications of adhesive joints include bonding metallic and composite body panels for automotive and aeronautical structures where light weight and high fatigue strength are prime requirements. Many theoretical and experimental studies have investigated the static and dynamic behaviors of

* Corresponding author.
E-mail address: hbrito@usp.br (H. Brito-Santana).

https://doi.org/10.1016/j.apm.2018.01.009
0307-904X/

adhesive joints [1–7]. In fact, the increasing use of composite laminates has stimulated advances in the analysis and design of this type of material. For example, rigid (perfect) bonding to ensure the continuity of all the field variables (stress and displacement components) has been considered in analytical and numerical studies of layered composite materials. However, from a more rigorous practical viewpoint, the existence of a perfect interfacial bond in a real layered composite seems almost impossible [8].

Several studies [9–13] have shown that epoxy-based adhesives form a so-called interphase in adhesive joints, and thus the term interphase to refer to an interlayer was used in the present work. Various studies [14–20] have described the influence of the interlayer in a phenomenological manner as a qualitative change in the mechanical and/or thermomechanical properties. For example, Geiss and Schumann studied an epoxy adhesive and proposed a method for predicting the local mechanical properties of polymer interlayers in structural adhesive joints [21]. As expected, the effective coefficients depend on the microstructures and properties of the layers, but also the interfacial bonding conditions. Thus, some studies have also simulated the mechanical behavior of layered composites with delamination. Theoretical studies of multilayered plates with imperfect interfaces have been reviewed extensively [22]. Massabò and Campi [23] proposed an extension of these theories to account for mixed-mode interfaces, as suggested by Librescu and Schmidt [24], and for affine (linear non-proportional) interfacial traction laws. Based on these extended theories, a homogenized approach was proposed for application to structures with generally nonlinear cohesive interfaces, where the cohesive traction laws can be approximated as piecewise linear functions of the relative displacements at the interfaces [25,26]. In addition, Takahashi et al. [27] suggested an optimum material selection and interlayer thickness for perfect ceramic-metal joint structures. However, all of these previous studies evaluated the mechanical behavior (displacements, and strain and stress fields) of layered composites or bonded joints by considering the presence or absence of defects, whereas they did not focus on the effective properties of interface effects (e.g., delamination) at the macro-scale level.

Moreover, many studies calculated the effective properties by considering the interface effect at the micro-scale level [28–32], *i.e.*, the influence of the interface between the fiber and matrix on the effective properties of a composite material. This effect can be illustrated using new material interface models proposed in various studies [33–39]. Another type of approach for modeling the interface was also suggested by Mal and Bose [40] and it was investigated in subsequent studies [41–51]. Thus, many studies have focused on the micro-scale level where various different approaches [52-65] have been proposed for analyzing perfect and imperfect adhesion with a uniform interface between the fiber and matrix. In particular, a mathematical framework was developed to predict the mechanical behavior of regularly inhomogeneous media under the assumption of an ordered microstructure in these media with perfect interfacial bonding [53–56]. Cherednichenko and Evans [57] proposed a two-scale asymptotic expansion and higher-order constitutive laws for the homogenization of a system of quasi-static Maxwell equations by considering a perfect contact interface. The interface between the fiber and matrix has also been modeled using a uniform spring damaged parameter [58–62]. Other studies considered model composites with inclusions surrounded by an interphase zone, where the properties were treated as graded in the radial direction [63–65]. Thus, many studies have determined the effective properties by regarding defects at the micro-scale level, *i.e.*, between the fiber and matrix.

Based on the previous studies mentioned above, in the present study, it was investigated the effective elastic properties of layered composites (at the macro-scale level) by considering the influence of non-uniform imperfect adhesion and by using interface models between the layers. These models are first verified at the micro-scale level [58], *i.e.*, by considering defects between the fiber and polymer matrix. In practical terms, the influence of non-uniform imperfection on the effective properties of layered composites is evaluated when delamination is present between the adjacent layers. In fact, a laminated composite with perfect contact between the layers and a periodic distribution between them was investigated by Brito-Santana et al. [66]. Thus, the present investigation is an extension of previous research [58,66]. It is important to note that the key feature of the present investigation compared with previous studies [22–66] is that it was considered the effect of delamination by using asymptotic expansion in the analytical approach. In particular, we develop the two scale asymptotic homogenization method (AHM) was developed for composites under an imperfect interface model by introducing the shear lag (or spring layer) model. Thus, the proposed model is different because it was assumed that a spring layer of distributed along the interface as a piecewise discontinuous function between the layers with delaminations. Moreover, it was stated the problem for a two-layer model with non-uniform imperfect adhesion (spring type) conditions and a three-layer composite material with perfect conditions between the layers based on the range of the two scale AHM. The associated local problems are derived, and thus the local functions are solved directly. In addition, using the two-layer model with imperfect interface conditions and the three-layer model with perfect conditions, analytical expressions for the interlayer properties were derived in the so-called interface model, and it was shown that the interlayer properties are related to the constituent properties and geometry. Finally, a composite structure with layers made from titanium Ti6Al4V [67] and ceramic AD-96 [68] was investigated by using perfect and imperfect interface models with different approaches. A representative volume element (RVE) is analyzed by using the finite element method (FEM) package Abaqus^{TM} to calculate the effective properties. In addition, two-scale AHM is employed to provide the analytical expression of the effective properties for the periodic layered composite. A very important motivation for the present study is employing analytical and numerical approaches as design tools to aid the development of composite structures by considering the interface damage between the layers. In particular, it was considered non-uniform imperfect adhesion in layered composites, which should be evaluated during certification processes for automotive, aeronautical, and other structures (e.g., wind turbines).

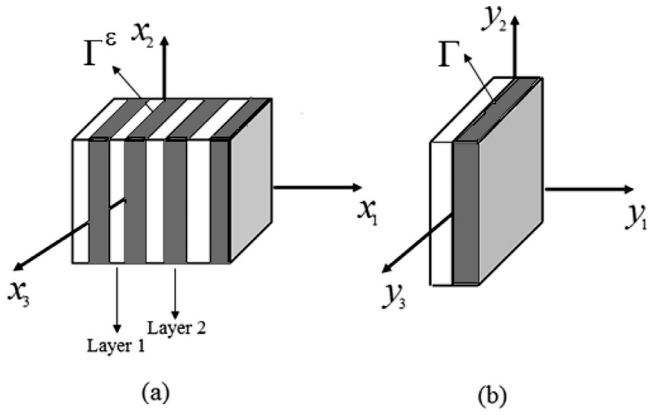

Fig. 1. Three-dimensional laminated composite and unit cell: (a) layered composite, and (b) unit cell.

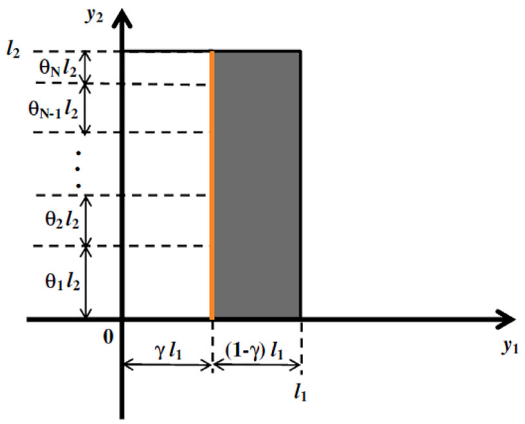

Fig. 2. Two-dimensional unit cell with non-uniform imperfect adhesion. $\sum_{r=1}^{N} \theta_r = 1$.

2. Formulation of the problem

2.1. Geometrical description

It was considered a periodically laminated composite similar to the structure defined by Brito-Santana et al. [66] but with non-uniform imperfect contact, which occupies a bounded region Ω^ε in $\mathbb{R}^3$ space with Lipschitz boundary $\partial\Omega^\varepsilon = \overline{\partial_1\Omega^\varepsilon} \cup \overline{\partial_2\Omega^\varepsilon}$ such that $\partial_1\Omega^\varepsilon \cap \partial_2\Omega^\varepsilon = \phi$, where $\partial_1\Omega^\varepsilon$ and $\partial_2\Omega^\varepsilon$ are boundary portions. It is assumed that the region Ω^ε comprises periodic repetitions of the unit cell Y in the parallelepiped form with dimensions $\varepsilon y_i (i = 1, 2, 3)$, where ε is the ratio of the unit cell size (*i.e.*, period of the structure) related to a typical length in the region. The AHM is presented for a periodically layered composite by considering non-uniform imperfect adhesion. Fig. 1 shows the three-dimensional layered composite, where Γ^ε is the interface separating the composite layers, which depends on the slow variable $\boldsymbol{x}$, and Γ is the interface in the unit cell, which depends on the fast variable $\boldsymbol{y}$. The medium is assumed to be layered in the x_1 direction, where all of the material parameters are independent of x_2 and x_3. Fig. 2 shows the two-dimensional unit cell with non-uniform interface adhesion, where $\theta_r l_2$ is the length of the r-partition with degree of imperfection θ_r "$r = 1,\ldots, N$" for the interface, and N is the number of partitions of the interface.

2.2. Statement of the problem

The problem is formulated in the bounded subset Ω^ε of $\mathbb{R}^3$, where $Y = \{\boldsymbol{y} = (y_1, y_2, y_3) \in \mathbb{R}^3 : 0 < y_i < l_i, i = 1, 2, 3\}$ denotes the reference cell and l_i are positive numbers. It is important to note that $\Omega^\varepsilon = \varepsilon Y = \{\boldsymbol{x} = (x_1, x_2, x_3) \in \mathbb{R}^3 : \varepsilon^{-1} x_i \in Y, i = 1, 2, 3\}$, where $\boldsymbol{y} = \boldsymbol{x}/\varepsilon$.

A general field variable f_i^ε now depends on both the macro- and micro-scale, $f_i^\varepsilon(\boldsymbol{x}) = f_i(\boldsymbol{x}, \boldsymbol{y})$, and the partial derivatives take the form:

$$\frac{\partial f_i^\varepsilon}{\partial x_j} = \frac{\partial f_i}{\partial x_j} + \varepsilon^{-1} \frac{\partial f_i}{\partial y_j}. \tag{1}$$

Assuming that the body forces are equal to zero, then the elastic equilibrium equation is given by

$$\frac{\partial \sigma_{ij}^{\varepsilon}}{\partial x_j} = 0 \text{ in } \Omega^{\varepsilon}, \tag{2}$$

$$\sigma_{ij}^{\varepsilon} n_j = K_{ij} \left\| u_j^{\varepsilon} \right\|_{\Gamma^{\varepsilon}} = \begin{cases} {}_1K_{ij} \left\| u_j^{\varepsilon} \right\|_{\Gamma_1^{\varepsilon}} \text{ in } Y_1 \\ \vdots \\ {}_NK_{ij} \left\| u_j^{\varepsilon} \right\|_{\Gamma_N^{\varepsilon}} \text{ in } Y_N \end{cases}, \left\| \sigma_{ij}^{\varepsilon} \right\|_{\Gamma^{\varepsilon}} n_j = \begin{cases} \left\| \sigma_{ij}^{\varepsilon} \right\|_{\Gamma_1^{\varepsilon}} n_j = 0 \text{ in } Y_1 \\ \vdots \\ \left\| \sigma_{ij}^{\varepsilon} \right\|_{\Gamma_N^{\varepsilon}} n_j = 0 \text{ in } Y_N \end{cases}, \text{ on } \Gamma^{\varepsilon} = \bigcup_{r=1}^{N} \Gamma_r^{\varepsilon}$$

$$K_{ij} = \begin{cases} {}_1K_{ij} \text{ in } Y_1 \\ \vdots \\ {}_NK_{ij} \text{ in } Y_N \end{cases}, \quad {}_rK_{ij} = 0, i \neq j; r = 1, 2, ..., N, \tag{3}$$

$$\sigma_{ij}^{\varepsilon} = C_{ijkl}(\boldsymbol{y}) \frac{\partial u_k^{\varepsilon}}{\partial x_l}, \tag{4}$$

where $\sigma_{ij}^{\varepsilon}$, u_i^{ε} are the components of the stress tensor and displacement vector, $\|\bullet\|$ denotes the jump across the interface, *i.e.*, $\|\bullet\| = (\bullet)^{(1)}(\boldsymbol{y}) - (\bullet)^{(2)}(\boldsymbol{y})$ for $\boldsymbol{y} \in \Gamma$, ${}_rK_{ij}$(GPa/mm) > 0 denotes the interface stiffness properties for the r-interface-partition Γ_r (where ${}_rK_{ij} \to \infty$ corresponds to a perfect interface), $C_{ijkl} = C_{ijkl}^{(1)}$ for $0 < y_1 < \gamma l_1$ and $C_{ijkl} = C_{ijkl}^{(2)}$ for $\gamma l_1 < y_1 < l_1$ (γ is the volume fraction of layer 1 and l_1 is the length of the unit cell in the x_1 direction), and n_j is the unit vector in the outward normal direction. The symbol Y_r (defined in (21)) represents the r-partition of the unit cell Y. In the following, the Latin indices take values of 1, 2 and 3. It is important to note that the proposed formulation focuses on linear interfaces represented by Eq. (3), and the $\boldsymbol{K}$ terms linking the tractions and the displacement jumps. However, it is possible to expand the concept to the more general case of nonlinear interfaces (e.g., cohesive interfaces) and to replace them using a nonlinear interphase layer with compatible interfaces. Thus, this approach may be a simpler or more accessible alternative for modeling non-uniform and degrading interface problems.

3. Homogenization

In this section, analytical and numerical homogenization procedures were based on the two-scale AHM and FEM, respectively. AHM is employed to homogenize system (2)–(4) and to derive the effective properties for layered composites by considering non-uniform imperfect adhesion. In addition, by combining the effective coefficients for the two-layer model with coefficients derived for the three-layer model, analytical expressions for the elastic interlayer are obtained, *i.e.*, the so-called interface model, which are used for computing the interface properties of the three-layer model by FEM.

3.1. Two scale AHM: two-layer elastic composite with an imperfect interface (spring type)

The heterogeneous medium with a microstructure at two length scales, *i.e.*, macroscopic "L" and microscopic "l" such that $L \gg l$, can be simulated by a homogeneous model with certain homogenized (so-called effective) properties. It is well known that under the assumptions of periodicity and the strict separation of scales, *i.e.*, in the regime where $l/L \to 0$ is a suitable approximation, the behavior of composites is fully determined by the solution of the so-called "cell problems" based on the period of the composite [57]. Scale effects can be analyzed systematically using the higher order AHM [59]. The theoretical foundations of AHM have been developed rigorously in previous studies [53–56].

The mechanical behavior of an imperfect interface is modeled via a layer of mechanical springs of zero thickness. The spring constants $K_n = K_{11}$, $K_t = K_{22} = K_{33} = K_s$ are normal and tangential interface stiffness properties. The infinite values of the parameters imply vanishing of the displacement jumps, and thus perfect interface conditions. At the other extremity, the zero values of the parameters imply vanishing of the interface tractions, and thus debonding. Any finite positive values for the interface parameters define an imperfect interface [61].

The displacements ($u_i^{\varepsilon}(\boldsymbol{x})$) is expressed in the form of the following two-scale asymptotic expansion [54–56]

$$u_i^{\varepsilon}(\boldsymbol{x}) = u_i^{(0)}(\boldsymbol{x}) + \varepsilon \cdot u_i^{(1)}(\boldsymbol{x}, \boldsymbol{y}) + \varepsilon^2 \cdot u_i^{(2)}(\boldsymbol{x}, \boldsymbol{y}) + \cdots. \tag{5}$$

By substituting (5) into (4), it is possible to obtain

$$\sigma_{ij}^{\varepsilon}(\boldsymbol{x}) = \sigma_{ij}^{(0)}(\boldsymbol{x}, \boldsymbol{y}) + \varepsilon \cdot \sigma_{ij}^{(1)}(\boldsymbol{x}, \boldsymbol{y}) + \varepsilon^2 \cdot \sigma_{ij}^{(2)}(\boldsymbol{x}, \boldsymbol{y}) + \cdots, \tag{6}$$

where

$$\sigma_{ij}^{(m)}(\boldsymbol{x}, \boldsymbol{y}) = C_{ijkl}(\boldsymbol{y}) \frac{\partial u_k^{(m)}}{\partial x_l} + C_{ijkl}(\boldsymbol{y}) \frac{\partial u_k^{(m+1)}}{\partial y_l} \; m = 0, 1, 2, \cdots. \tag{7}$$

By substituting Eqs. (5) and (6) into (2), and rearranging the terms of the equal exponent ε, for ε^{-1} and ε^{0}, it is obtained the following equations

$$\frac{\partial \sigma_{ij}^{(0)}}{\partial y_j} = 0, \tag{8}$$

$$\frac{\partial \sigma_{ij}^{(0)}}{\partial x_j} + \frac{\partial \sigma_{ij}^{(1)}}{\partial y_j} = 0. \tag{9}$$

Using Eq. (7) for $m=0$ and Eq. (8), then

$$\frac{\partial}{\partial y_j}\left(C_{ijkl}\frac{\partial u_k^{(1)}}{\partial y_l}\right) = -\frac{\partial C_{ijkl}}{\partial y_j}\frac{\partial u_k^{(0)}}{\partial x_l}, \tag{10}$$

where the solution is represented in the form of

$$u_i^{(1)}(\boldsymbol{x},\boldsymbol{y}) = N_{ijk}^{2\mathrm{AHM}}(\boldsymbol{y})\frac{\partial u_j^{(0)}(\boldsymbol{x})}{\partial x_k}, \tag{11}$$

and thus it was obtained the following local problems for determining the l_1-periodic auxiliary functions $N_{ijk}^{2\mathrm{AHM}}(\boldsymbol{y})$, and the notation 2AHM is associated with the two-layer spring problem

$$\frac{\partial}{\partial y_j}\left(C_{ijkl}\frac{\partial N_{kpq}^{2\mathrm{AHM}}}{\partial y_l} + C_{ijpq}\right) = 0 \text{ in } Y, \tag{12}$$

with interface conditions

$$\left(C_{ijkl}\frac{\partial N_{kpq}^{2\mathrm{AHM}}}{\partial y_l} + C_{ijpq}\right)n_j = K_{ij}\left\|N_{jpq}^{2\mathrm{AHM}}\right\|, \quad \left\|C_{ijkl}\frac{\partial N_{kpq}^{2\mathrm{AHM}}}{\partial y_l} + C_{ijpq}\right\|n_j = 0 \text{ on } \Gamma, \tag{13}$$

where the auxiliary functions $N_{ijk}^{2\mathrm{AHM}}(\boldsymbol{y})$ are piecewise linear functions in each unit cell portion Y_r and they are defined as

$$N_{kpq}^{2\mathrm{AHM}} = \begin{cases} {}_1N_{kpq}^{2\mathrm{AHM}} \text{ in } Y_1 \\ \vdots \\ {}_NN_{kpq}^{2\mathrm{AHM}} \text{ in } Y_N \end{cases}, \tag{14}$$

with the r-interface-partition local functions ${}_rN_{ijk}^{2\mathrm{AHM}}$ ($r=1, ..., N$).

The existence of the local functions $N_{kpq}^{2\mathrm{AHM}}$ is guaranteed up to an additive constant (*cf.* Lemma 1 in [56]). To ensure the uniqueness, it is taken $N_{kpq}^{2\mathrm{AHM}}$ such that $\langle N_{kpq}^{2\mathrm{AHM}}\rangle_Y = 0$. The cell average operator $\langle\bullet\rangle_Y$ is defined as $\langle\bullet\rangle_Y = \frac{1}{|Y|}\int_Y \bullet\, dY$, where $|Y|$ is the unit cell volume.

From Eq. (7), for $m=0$ and considering (11), it is obtained

$$\sigma_{ij}^{(0)} = \left(C_{ijpq} + C_{ijkl}\frac{\partial N_{kpq}^{2\mathrm{AHM}}}{\partial y_l}\right)\frac{\partial u_p^{(0)}}{\partial x_q}. \tag{15}$$

The macroscopic equilibrium equation is obtained by averaging Eq. (9), and thus

$$\frac{\partial \left\langle \sigma_{ij}^{(0)}\right\rangle_Y}{\partial x_j} = 0, \tag{16}$$

where

$$\left\langle \sigma_{ij}^{(0)}\right\rangle_Y = \frac{1}{|Y|}\int_V \sigma_{ij}^{(0)}\, dY = C_{ijkl}^{*}\frac{\partial u_k^{(0)}}{\partial x_l}, \tag{17}$$

with

$$C_{ijkl}^{*} = \left\langle C_{ijkl} + C_{ijhs}\frac{\partial N_{hkl}^{2\mathrm{AHM}}}{\partial y_s}\right\rangle_Y. \tag{18}$$

Proposition. *Expression (18) for the effective moduli C_{ijkl}^{*} can be written as*

$$C_{ijkl}^{*} = \sum_{r=1}^{N}\theta_r\left\langle C_{ijkl} + C_{ijh1}\frac{\partial_r N_{hkl}^{2\mathrm{AHM}}}{\partial y_1}\right\rangle_{Y_r},$$

where θ_r denotes the degree of imperfection for the r-partition.

Proof. Considering (18) and (14), it is possible to have

$$C^*_{ijkl} = \left\langle C_{ijkl} + C_{ijhs}\frac{\partial N^{2AHM}_{hkl}}{\partial y_s}\right\rangle_Y = \frac{1}{l_1 l_2}\int_0^{l_1}\int_0^{l_2}\left(C_{ijkl} + C_{ijhs}\frac{\partial N^{2AHM}_{hkl}}{\partial y_s}\right)dy_1 dy_2,$$

$$C^*_{ijkl} = \frac{1}{l_1 l_2}\sum_{r=1}^{N}\int_0^{l_1}\int_0^{\theta_r l_2}\left(C_{ijkl} + C_{ijhs}\frac{\partial_r N^{2AHM}_{hkl}}{\partial y_s}\right)dy_1 dy_2 = \sum_{r=1}^{N}\frac{\theta_r}{l_1}\int_0^{l_1}\left(C_{ijkl} + C_{ijhs}\frac{\partial_r N^{2AHM}_{hkl}}{\partial y_s}\right)dy_1,$$

and finally, it is possible to obtain

$$C^*_{ijkl} = \sum_{r=1}^{N}\frac{\theta_r}{l_1}\int_0^{l_1}\left(C_{ijkl} + C_{ijhs}\frac{\partial_r N^{2AHM}_{hkl}}{\partial y_s}\right)dy_1 = \sum_{r=1}^{N}\theta_r\left\langle C_{ijkl} + C_{ijh1}\frac{\partial_r N^{2AHM}_{hkl}}{\partial y_1}\right\rangle_{Y_r}. \qquad \square$$

From (12), (13) and using (14), we obtain the following local problems for each r-interface-partition:

$$\frac{\partial}{\partial y_j}\left(C_{ijkl}\frac{\partial_r N^{2AHM}_{kpq}}{\partial y_l} + C_{ijpq}\right) = 0 \text{ in } Y_r, \tag{19}$$

with the interface conditions

$$\left(C_{ijkl}\frac{\partial_r N^{2AHM}_{kpq}}{\partial y_l} + C_{ijpq}\right)n_j = {}_rK_{ij}\left\|{}_rN^{2AHM}_{jpq}\right\|, \left\|C_{ijkl}\frac{\partial_r N^{2AHM}_{kpq}}{\partial y_l} + C_{ijpq}\right\|n_j = 0 \text{ on } \Gamma_r. \tag{20}$$

where

$$Y_r = \left\{\boldsymbol{y} = (y_1, y_2, y_3) \in \mathbb{R}^3 : 0 < y_i < l_i, i = 1,3 \text{ and } l_2\sum_{i=0}^{r-1}\theta_i < y_2 < l_2\sum_{i=1}^{r}\theta_i, \theta_0 = 0\right\}, \tag{21}$$

and Γ_r is the interface of the unit cell portion Y_r.

The medium is assumed to be layered in the x_1 direction, so the elastic moduli C_{ijkl} only depend on $y_1 = x_1/\varepsilon$, and Eq. (19) takes the form

$$\frac{d}{dy_1}\left(C_{i1k1}\frac{d_r N^{2AHM}_{kpq}}{dy_1} + C_{i1pq}\right) = 0 \text{ in } Y_r, \tag{22}$$

with the interface conditions

$$\left(C_{i1k1}\frac{d_r N^{2AHM}_{kpq}}{dy_1} + C_{i1pq}\right)n_1 = {}_rK_{im}\left\|{}_rN^{2AHM}_{mpq}\right\|, \left\|C_{i1k1}\frac{d_r N^{2AHM}_{kpq}}{dy_1} + C_{i1pq}\right\|n_1 = 0 \text{ on } \Gamma_r, \tag{23}$$

where integration gives

$$C_{i1k1}\frac{d_r N^{2AHM}_{kpq}}{dy_1} + C_{i1pq} = {}_rA^{2AHM}_{ipq}, \tag{24}$$

or

$$\frac{d_r N^{2AHM}_{kpq}}{dy_1} = (C_{k1i1})^{-1}\,{}_rA^{2AHM}_{ipq} - (C_{k1i1})^{-1}C_{i1pq}, \tag{25}$$

where $(C_{k1i1})^{-1}$ are the components of the inverse to the tensor of the second rank $\tilde{\boldsymbol{C}} = C_{i1k1}\,\boldsymbol{e}_i \otimes \boldsymbol{e}_k$ and ${}_rA^{2AHM}_{ipq}$ is independent of variable y_1.

By averaging Eq. (25), it is possible to obtain

$$\left\langle\frac{d_r N^{2AHM}_{kpq}}{dy_1}\right\rangle_{Y_r} = \frac{1}{l_1}\lim_{\substack{h\to 0\\ h>0}}\left(\int_0^{\gamma l_1 - h}\frac{d_r N^{2AHM}_{kpq}}{dy_1}dy_1 + \int_{\gamma l_1 + h}^{l_1}\frac{d_r N^{2AHM}_{kpq}}{dy_1}dy_1\right) = -\left\langle(C_{k1i1})^{-1}C_{i1pq}\right\rangle_{Y_r} + \left\langle(C_{k1i1})^{-1}\right\rangle_{Y_r}{}_rA^{2AHM}_{ipq},$$

$$\frac{1}{l_1}\lim_{\substack{h\to 0\\ h>0}}\left({}_rN^{2AHM}_{kpq}(\gamma l_1 - h) - {}_rN^{2AHM}_{kpq}(\gamma l_1 + h)\right) + \frac{1}{l_1}{}_rN^{2AHM}_{kpq}(l_1) - \frac{1}{l_1}{}_rN^{2AHM}_{kpq}(0)$$

$$= -\left\langle(C_{k1i1})^{-1}C_{i1pq}\right\rangle_{Y_r} + \left\langle(C_{k1i1})^{-1}\right\rangle_{Y_r}{}_rA^{2AHM}_{ipq}. \tag{26}$$

By considering the periodicity of ${}_rN^{2AHM}_{kpq}$ and the definition of $\|\bullet\|$, Eq. (26) can be rewritten as

$$\frac{1}{l_1}\left|\left|{}_rN^{2AHM}_{kpq}\right|\right| = -\langle(C_{k1i1})^{-1}C_{i1pq}\rangle_{Y_r} + \langle(C_{k1i1})^{-1}\rangle_{Y_r}{}_rA^{2AHM}_{ipq}. \tag{27}$$

Evaluating Eq. (24) on the interface Γ_r and combining with condition $(23)_1$, it is possible to have

$$\left|\left|{}_rN^{2AHM}_{mpq}\right|\right| = -({}_rK_{mi})^{-1}\,{}_rA^{2AHM}_{ipq}, \tag{28}$$

where $({}_rK_{ij})^{-1}$ are the components of the tensor inverse to the tensor ${}_r\tilde{\boldsymbol{K}} = {}_rK_{ij}\,\boldsymbol{e}_i \otimes \boldsymbol{e}_j$.

By substituting (28) into (27), it is obtained

$$ {}_rA^{2AHM}_{ipq} = \left\langle (C_{i1m1})^{-1} \right\rangle^{-1}_{Y_r} \left\langle (C_{m1s1})^{-1}\, C_{s1pq} \right\rangle_{Y_r}, \tag{29} $$

where

$$ \left\langle (C_{i1m1})^{-1} \right\rangle^{-1}_{Y_r} = \left[\gamma \left(C^{(1)}_{i1m1}\right)^{-1} + (1-\gamma)\left(C^{(2)}_{i1m1}\right)^{-1} + \frac{({}_rK_{im})^{-1}}{l_1} \right]^{-1}, $$

and

$$ \left\langle (C_{m1s1})^{-1}\, C_{s1pq} \right\rangle_{Y_r} = \gamma \left(C^{(1)}_{m1s1}\right)^{-1} C^{(1)}_{s1pq} + (1-\gamma)\left(C^{(2)}_{m1s1}\right)^{-1} C^{(2)}_{s1pq}. $$

The solution to Eq. (24) can be written as

$$ {}_rN^{2AHM}_{kpq} = {}_rB^{2AHM}_{kpq} - \left\langle {}_rB^{2AHM}_{kpq} \right\rangle, \tag{30} $$

where

$$ {}_rB^{2AHM}_{kpq} = \int_0^{y_1} \left((C_{k1i1})^{-1}\, {}_rA^{2AHM}_{ipq} - (C_{k1i1})^{-1} C_{i1pq} \right) d\xi. \tag{31} $$

The expression of the local functions ${}_rN^{2AHM}_{kpq}$ is

$$ {}_rN^{2AHM}_{kpq} = \begin{cases} {}_rB^{2AHM}_{kpq(1)}\, y_1 - \left\langle {}_rB^{2AHM}_{kpq} \right\rangle, & 0 < y_1 < \gamma\, l_1 \\ {}_rB^{2AHM}_{kpq(2)}\, (y_1 - \gamma\, l_1) + {}_rB^{2AHM}_{kpq(3)} - \left\langle {}_rB^{2AHM}_{kpq} \right\rangle, & \gamma\, l_1 < y_1 < l_1 \end{cases}, \tag{32} $$

with

$$ {}_rB^{2AHM}_{kpq(s)} = \left(C^{(s)}_{k1i1}\right)^{-1} {}_rA^{2AHM}_{ipq} - \left(C^{(s)}_{k1i1}\right)^{-1} C^{(s)}_{i1pq},\ s = 1, 2,\ {}_rB^{2AHM}_{kpq(3)} = \gamma\, l_1 B^{2AHM}_{kpq(1)} + ({}_rK_{ki})^{-1}\, {}_rA^{2AHM}_{ipq}, $$

$$ {}_rA^{2AHM}_{ipq} = \left[\gamma \left(C^{(1)}_{i1m1}\right)^{-1} + (1-\gamma)\left(C^{(2)}_{i1m1}\right)^{-1} + \frac{({}_rK_{im})^{-1}}{l_1} \right]^{-1} \left[\gamma \left(C^{(1)}_{m1s1}\right)^{-1} C^{(1)}_{s1pq} + (1-\gamma)\left(C^{(2)}_{m1s1}\right)^{-1} C^{(2)}_{s1pq} \right], $$

and

$$ \left\langle {}_rB^{2AHM}_{kpq} \right\rangle = \frac{\gamma^2 l_1\, {}_rB^{2AHM}_{kpq(1)}}{2} + \frac{(1-\gamma)^2 l_1\, {}_rB^{2AHM}_{kpq(2)}}{2} + (1-\gamma)\, {}_rB^{2AHM}_{kpq(3)}. $$

The detailed expressions of the non-zero local functions ${}_rN^{2AHM}_{kpq}$ for isotropic constituents are

$$ {}_rN^{2AHM}_{111} = \begin{cases} {}_rB^{2AHM}_{111(1)}\, y_1 - \left\langle {}_rB^{2AHM}_{111} \right\rangle, & 0 < y_1 < \gamma\, l_1 \\ {}_rB^{2AHM}_{111(2)}\, (y_1 - \gamma\, l_1) + {}_rB^{2AHM}_{111(3)} - \left\langle {}_rB^{2AHM}_{111} \right\rangle, & \gamma\, l_1 < y_1 < l_1 \end{cases}, \tag{33} $$

where

$$ {}_rB^{2AHM}_{111(s)} = \frac{{}_rA^{2AHM}_{111}}{C^{(s)}_{1111}} - 1,\ s = 1, 2,\ {}_rB^{2AHM}_{111(3)} = \gamma\, l_1\, {}_rB^{2AHM}_{111(1)} + \frac{{}_rA^{2AHM}_{111}}{{}_rK_n}, $$

$$ {}_rA^{2AHM}_{111} = \frac{C^{(1)}_{1111} C^{(2)}_{1111}\, l_1\, {}_rK_n}{\left[(1-\gamma) C^{(1)}_{1111} + \gamma C^{(2)}_{1111} \right] l_1\, {}_rK_n + C^{(1)}_{1111} C^{(2)}_{1111}}, $$

and

$$ \left\langle {}_rB^{2AHM}_{111} \right\rangle = \frac{\gamma^2 l_1\, {}_rB^{2AHM}_{111(1)}}{2} + \frac{(1-\gamma)^2 l_1\, {}_rB^{2AHM}_{111(2)}}{2} + (1-\gamma)\, {}_rB^{2AHM}_{111(3)}. $$

$$ {}_rN^{2AHM}_{122} = {}_rN^{2AHM}_{133} = \begin{cases} {}_rB^{2AHM}_{122(1)}\, y_1 - \left\langle {}_rB^{2AHM}_{122} \right\rangle, & 0 < y_1 < \gamma\, l_1 \\ {}_rB^{2AHM}_{122(2)}\, (y_1 - \gamma\, l_1) + {}_rB^{2AHM}_{122(3)} - \left\langle {}_rB^{2AHM}_{122} \right\rangle, & \gamma\, l_1 < y_1 < l_1 \end{cases}, \tag{34} $$

with

$$ {}_rB^{2AHM}_{122(s)} = \frac{{}_rA^{2AHM}_{122} - C^{(s)}_{1122}}{C^{(s)}_{1111}},\ s = 1, 2,\ {}_rB^{2AHM}_{122(3)} = \gamma\, l_1\, {}_rB^{2AHM}_{122(1)} + \frac{{}_rA^{2AHM}_{122}}{{}_rK_n}, $$

$$ {}_rA^{2AHM}_{122} = \frac{\left[(1-\gamma) C^{(1)}_{1111} C^{(2)}_{1122} + \gamma C^{(2)}_{1111} C^{(1)}_{1122} \right] l_1\, {}_rK_n}{\left[(1-\gamma) C^{(1)}_{1111} + \gamma C^{(2)}_{1111} \right] l_1\, {}_rK_n + C^{(1)}_{1111} C^{(2)}_{1111}}, $$

and

$$\left\langle {}_rB_{122}^{2AHM}\right\rangle = \frac{\gamma^2 l_1 {}_rB_{122(1)}^{2AHM}}{2} + \frac{(1-\gamma)^2 l_1 {}_rB_{122(2)}^{2AHM}}{2} + (1-\gamma){}_rB_{122(3)}^{2AHM}.$$

$$\begin{aligned} {}_rN_{212}^{2AHM} &= {}_rN_{221}^{2AHM} = {}_rN_{313}^{2AHM} \\ &= {}_rN_{331}^{2AHM} = \begin{cases} {}_rB_{212(1)}^{2AHM}\, y_1 - \left\langle {}_rB_{212}^{2AHM}\right\rangle, & 0 < y_1 < \gamma\, l_1 \\ {}_rB_{212(2)}^{2AHM}\,(y_1 - \gamma\, l_1) + {}_rB_{212(3)}^{2AHM} - \left\langle {}_rB_{212}^{2AHM}\right\rangle, & \gamma\, l_1 < y_1 < l_1 \end{cases}, . \end{aligned} \tag{35}$$

where

$${}_rB_{212(s)}^{2AHM} = \frac{{}_rA_{212}^{2AHM}}{C_{1212}^{(s)}} - 1,\ s = 1, 2,\ {}_rB_{212(3)}^{2AHM} = \gamma l_1 {}_rB_{212(1)}^{2AHM} + \frac{{}_rA_{212}^{2AHM}}{{}_rK_t},$$

$${}_rA_{212}^{2AHM} = \frac{C_{1212}^{(1)} C_{1212}^{(2)} l_1 {}_rK_t}{\left[(1-\gamma)C_{1212}^{(1)} + \gamma C_{1212}^{(2)}\right] l_1 {}_rK_t + C_{1212}^{(1)} C_{1212}^{(2)}},$$

and

$$\left\langle {}_rB_{212}^{2AHM}\right\rangle = \frac{\gamma^2 l_1 {}_rB_{212(1)}^{2AHM}}{2} + \frac{(1-\gamma)^2 l_1 {}_rB_{212(2)}^{2AHM}}{2} + (1-\gamma){}_rB_{212(3)}^{2AHM}.$$

The non-zero local functions ${}_rN_{ijk}^{2AHM}$ are calculated for isotropic constituents and by using Eq. (18), the effective moduli can be written as

$$\begin{aligned} C_{1111}^{*2AHM} &= \sum_{r=1}^{N} \theta_r \left\langle \frac{1}{C_{1111}} \right\rangle_{Y_r}^{-1},\ C_{1122}^{*2AHM} = C_{1133}^{*2AHM} = \sum_{r=1}^{N} \theta_r \left\langle \frac{1}{C_{1111}} \right\rangle_{Y_r}^{-1} \left\langle \frac{C_{1122}}{C_{1111}} \right\rangle_{Y_r}, \\ C_{2222}^{*2AHM} &= C_{3333}^{*2AHM} = \sum_{r=1}^{N} \theta_r \left(\langle C_{1111} \rangle_{Y_r} + \left\langle \frac{1}{C_{1111}} \right\rangle_{Y_r}^{-1} \left\langle \frac{C_{1122}}{C_{1111}} \right\rangle_{Y_r}^{2} - \left\langle \frac{(C_{1122})^2}{C_{1111}} \right\rangle_{Y_r} \right), \\ C_{2233}^{*2AHM} &= \sum_{r=1}^{N} \theta_r \left(\langle C_{1122} \rangle_{Y_r} + \left\langle \frac{1}{C_{1111}} \right\rangle_{Y_r}^{-1} \left\langle \frac{C_{1122}}{C_{1111}} \right\rangle_{Y_r}^{2} - \left\langle \frac{(C_{1122})^2}{C_{1111}} \right\rangle_{Y_r} \right), \\ C_{1212}^{*2AHM} &= C_{1313}^{*2AHM} = \sum_{r=1}^{N} \theta_r \left\langle \frac{1}{C_{1111}} \right\rangle_{Y_r}^{-1}, C_{2323}^{*2AHM} = \frac{1}{2}\left[C_{2222}^{*2AHM} - C_{2233}^{*2AHM}\right], \end{aligned} \tag{36}$$

where

$$\left\langle \frac{1}{C_{1111}} \right\rangle_{Y_r}^{-1} = \frac{C_{1111}^{(1)} C_{1111}^{(2)} l_1 {}_rK_n}{\left[(1-\gamma)C_{1111}^{(1)} + \gamma C_{1111}^{(2)}\right] l_1 {}_rK_n + C_{1111}^{(1)} C_{1111}^{(2)}},$$

$$\left\langle \frac{C_{1122}}{C_{1111}} \right\rangle_{Y_r} = \frac{(1-\gamma)C_{1111}^{(1)} C_{1122}^{(2)} + \gamma C_{1111}^{(2)} C_{1122}^{(1)}}{C_{1111}^{(1)} C_{1111}^{(2)}},\ \left\langle \frac{(C_{1122})^2}{C_{1111}} \right\rangle_{Y_r} = \frac{(1-\gamma)C_{1111}^{(1)} \left(C_{1122}^{(2)}\right)^2 + \gamma C_{1111}^{(2)} \left(C_{1122}^{(1)}\right)^2}{C_{1111}^{(1)} C_{1111}^{(2)}},$$

$$\left\langle \frac{1}{C_{1212}} \right\rangle_{Y_r}^{-1} = \frac{C_{1212}^{(1)} C_{1212}^{(2)} l_1 {}_rK_t}{\left[(1-\gamma)C_{1212}^{(1)} + \gamma C_{1212}^{(2)}\right] l_1 {}_rK_t + C_{1212}^{(1)} C_{1212}^{(2)}},\ \left\langle C_{ijkl} \right\rangle_{Y_r} = \gamma C_{ijkl}^{(1)} + (1-\gamma) C_{ijkl}^{(2)}.$$

It should be noted that the effective coefficient C_{1212}^{*} is a function of the tangential interface parameter K_t, whereas the other coefficients depend on the normal interface parameter K_n.

3.2. Two scale AHM: three-layer elastic composite with a perfect interface

Three-layer composites comprise an interlayer between two layers. The superscripts are assumed to be 1, *I* and 2 for the layer 1 interlayer (mesophase) and layer 2, respectively. The notation of 3AHM is associated with the three-layer problem.

Again, it was assumed that the medium is layered along x_1. The equation for the r-interface-partition local problem for the three-phase elastic composite with perfect adhesion is

$$\frac{d}{dy_1}\left(C_{i1k1} \frac{d_r N_{kpq}^{3AHM}}{dy_1} + C_{i1pq} \right) = 0 \text{ in } Y_r, \tag{37}$$

under interface conditions

$$\left\| {}_rN_{kpq}^{3AHM} \right\| = 0,\ \left\| C_{i1k1} \frac{d_r N_{kpq}^{3AHM}}{dy_1} + C_{i1pq} \right\| n_1 = 0 \text{ on } \Gamma_r. \tag{38}$$

The solution to problem (37) and (38) is obtained using the same method applied to the two-layer problem (22) and (23). The expression for the local functions ${}_rN^{3AHM}_{kpq}$ is

$$ {}_rN^{3AHM}_{kpq} = \begin{cases} {}_rB^{3AHM}_{kpq(1)}\, y_1 - \left\langle {}_rB^{3AHM}_{kpq}\right\rangle, & 0 < y_1 < \mathrm{v}^{(1)} l_1 \\ {}_rB^{3AHM}_{kpq(2)} \left(y_1 - \mathrm{v}^{(1)} l_1\right) + \mathrm{v}^{(1)} l_1 {}_rB^{3AHM}_{kpq(1)} - \left\langle {}_rB^{3AHM}_{kpq}\right\rangle, & \mathrm{v}^{(1)} l_1 < y_1 < \left(\mathrm{v}^{(1)} + \mathrm{v}^{(I)}\right) l_1 \\ {}_rB^{3AHM}_{kpq(3)} \left[y_1 - \left(\mathrm{v}^{(1)} + \mathrm{v}^{(I)}\right) l_1\right] + \mathrm{v}^{(I)} l_1 {}_rB^{3AHM}_{kpq(2)} + \mathrm{v}^{(1)} l_1 {}_rB^{3AHM}_{kpq(1)} - \left\langle {}_rB^{3AHM}_{kpq}\right\rangle, & \left(\mathrm{v}^{(1)} + \mathrm{v}^{(I)}\right) l_1 < y_1 < l_1 \end{cases}, \tag{39} $$

with

$$ {}_rB^{3AHM}_{kpq(s)} = \left(C^{(s)}_{k1m1}\right)^{-1} A^{3AHM}_{mpq} - \left(C^{(s)}_{k1m1}\right)^{-1} C^{(s)}_{m1pq},\ s = 1,2,3,\ {}_rA^{3AHM}_{mpq} = \left\langle \left(C_{m1i1}\right)^{-1}\right\rangle^{-1} \left\langle \left(C_{i1j1}\right)^{-1} C_{j1pq}\right\rangle, $$

$$ \left\langle {}_rB^{3AHM}_{kpq}\right\rangle = \frac{\left(\mathrm{v}^{(1)}\right)^2 l_1 {}_rB^{3AHM}_{kpq(1)}}{2} + \frac{\left(\mathrm{v}^{(I)}\right)^2 l_1 {}_rB^{3AHM}_{kpq(2)}}{2} + \frac{\left(\mathrm{v}^{(2)}\right)^2 l_1 {}_rB^{3AHM}_{kpq(3)}}{2} + \left(\mathrm{v}^{(1)}\mathrm{v}^{(I)} + \mathrm{v}^{(1)}\mathrm{v}^{(2)}\right) l_1 {}_rB^{3AHM}_{kpq(1)} + \mathrm{v}^{(I)}\mathrm{v}^{(2)} l_1 {}_rB^{3AHM}_{kpq(2)}. $$

and $\mathrm{v}^{(1)}$, $\mathrm{v}^{(I)}$, $\mathrm{v}^{(2)}$ are the layer 1, interlayer, and layer 2 volume fractions, respectively.

The detailed expressions for the non-zero local functions ${}_rN^{3AHM}_{kpq}$ for isotropic constituents are

$$ {}_rN^{3AHM}_{111} = \begin{cases} {}_rB^{3AHM}_{111(1)}\, y_1 - \left\langle {}_rB^{3AHM}_{111}\right\rangle, & 0 < y_1 < \mathrm{v}^{(1)} l_1 \\ {}_rB^{3AHM}_{111(2)} \left(y_1 - \mathrm{v}^{(1)} l_1\right) + \mathrm{v}^{(1)} l_1 {}_rB^{3AHM}_{111(1)} - \left\langle {}_rB^{3AHM}_{111}\right\rangle, & \mathrm{v}^{(1)} l_1 < y_1 < \left(\mathrm{v}^{(1)} + \mathrm{v}^{(I)}\right) l_1 \\ {}_rB^{3AHM}_{111(3)} \left[y_1 - \left(\mathrm{v}^{(1)} + \mathrm{v}^{(I)}\right) l_1\right] + \mathrm{v}^{(I)} l_1 {}_rB^{3AHM}_{111(2)} + \mathrm{v}^{(1)} l_1 {}_rB^{3AHM}_{111(1)} - \left\langle {}_rB^{3AHM}_{111}\right\rangle, & \left(\mathrm{v}^{(1)} + \mathrm{v}^{(I)}\right) l_1 < y_1 < l_1 \end{cases}, \tag{40} $$

where

$$ {}_rB^{3AHM}_{111(s)} = \frac{{}_rA^{3AHM}_{111}}{C^{(s)}_{1111}} - 1,\ s = 1,2,3,\ {}_rA^{3AHM}_{111} = \frac{C^{(1)}_{1111} {}_rC^{(I)}_{1111} C^{(2)}_{1111}}{\mathrm{v}^{(2)} C^{(1)}_{1111} {}_rC^{(I)}_{1111} + \mathrm{v}^{(I)} C^{(1)}_{1111} C^{(2)}_{1111} + \mathrm{v}^{(1)} {}_rC^{(I)}_{1111} C^{(2)}_{1111}}, $$

$$ \left\langle {}_rB^{3AHM}_{111}\right\rangle = \frac{\left(\mathrm{v}^{(1)}\right)^2 l_1 {}_rB^{3AHM}_{111(1)}}{2} + \frac{\left(\mathrm{v}^{(I)}\right)^2 l_1 {}_rB^{3AHM}_{111(2)}}{2} + \frac{\left(\mathrm{v}^{(2)}\right)^2 l_1 {}_rB^{3AHM}_{111(3)}}{2} + \left(\mathrm{v}^{(1)}\mathrm{v}^{(I)} + \mathrm{v}^{(1)}\mathrm{v}^{(2)}\right) l_1 {}_rB^{3AHM}_{111(1)} + \mathrm{v}^{(I)}\mathrm{v}^{(2)} l_1 {}_rB^{3AHM}_{111(2)}. $$

$$ {}_rN^{3AHM}_{122} = {}_rN^{3AHM}_{133} = \begin{cases} {}_rB^{3AHM}_{122(1)}\, y_1 - \left\langle {}_rB^{3AHM}_{122}\right\rangle, & 0 < y_1 < \mathrm{v}^{(1)} l_1 \\ {}_rB^{3AHM}_{122(2)} \left(y_1 - \mathrm{v}^{(1)} l_1\right) + \mathrm{v}^{(1)} l_1 {}_rB^{3AHM}_{122(1)} - \left\langle {}_rB^{3AHM}_{122}\right\rangle, & \mathrm{v}^{(1)} l_1 < y_1 < \left(\mathrm{v}^{(1)} + \mathrm{v}^{(I)}\right) l_1 \\ {}_rB^{3AHM}_{122(3)} \left[y_1 - \left(\mathrm{v}^{(1)} + \mathrm{v}^{(I)}\right) l_1\right] + \mathrm{v}^{(I)} l_1 {}_rB^{3AHM}_{122(2)} + \mathrm{v}^{(1)} l_1 {}_rB^{3AHM}_{122(1)} - \left\langle {}_rB^{3AHM}_{122}\right\rangle, & \left(\mathrm{v}^{(1)} + \mathrm{v}^{(I)}\right) l_1 < y_1 < l_1 \end{cases}, \tag{41} $$

with

$$ {}_rB^{3AHM}_{122(s)} = \frac{{}_rA^{3AHM}_{122} - C^{(s)}_{1122}}{C^{(s)}_{1111}},\ s = 1,2,3, $$

$$ {}_rA^{3AHM}_{122} = \frac{\mathrm{v}^{(2)} C^{(1)}_{1111} {}_rC^{(I)}_{1111} C^{(2)}_{1122} + \mathrm{v}^{(I)} C^{(1)}_{1111} C^{(2)}_{1111} {}_rC^{(I)}_{1122} + \mathrm{v}^{(1)} {}_rC^{(I)}_{1111} C^{(2)}_{1111} C^{(1)}_{1122}}{\mathrm{v}^{(2)} C^{(1)}_{1111} {}_rC^{(I)}_{1111} + \mathrm{v}^{(I)} C^{(1)}_{1111} C^{(2)}_{1111} + \mathrm{v}^{(1)} {}_rC^{(I)}_{1111} C^{(2)}_{1111}}, $$

$$ \left\langle {}_rB^{3AHM}_{122}\right\rangle = \frac{\left(\mathrm{v}^{(1)}\right)^2 l_1 {}_rB^{3AHM}_{122(1)}}{2} + \frac{\left(\mathrm{v}^{(I)}\right)^2 l_1 {}_rB^{3AHM}_{122(2)}}{2} + \frac{\left(\mathrm{v}^{(2)}\right)^2 l_1 {}_rB^{3AHM}_{122(3)}}{2} + \left(\mathrm{v}^{(1)}\mathrm{v}^{(I)} + \mathrm{v}^{(1)}\mathrm{v}^{(2)}\right) l_1 {}_rB^{3AHM}_{122(1)} + \mathrm{v}^{(I)}\mathrm{v}^{(2)} l_1 {}_rB^{3AHM}_{122(2)}. $$

$$ {}_rN^{3AHM}_{212} = {}_rN^{3AHM}_{221} = {}_rN^{3AHM}_{313} = {}_rN^{3AHM}_{331} = \begin{cases} {}_rB^{3AHM}_{212(1)}\, y_1 - \left\langle {}_rB^{3AHM}_{212}\right\rangle, & 0 < y_1 < \mathrm{v}^{(1)} l_1 \\ {}_rB^{3AHM}_{212(2)} \left(y_1 - \mathrm{v}^{(1)} l_1\right) + \mathrm{v}^{(1)} l_1 {}_rB^{3AHM}_{212(1)} - \left\langle {}_rB^{3AHM}_{212}\right\rangle, & \mathrm{v}^{(1)} l_1 < y_1 < \left(\mathrm{v}^{(1)} + \mathrm{v}^{(I)}\right) l_1 \\ {}_rB^{3AHM}_{212(3)} \left[y_1 - \left(\mathrm{v}^{(1)} + \mathrm{v}^{(I)}\right) l_1\right] + \mathrm{v}^{(I)} l_1 {}_rB^{3AHM}_{212(2)} + \mathrm{v}^{(1)} l_1 {}_rB^{3AHM}_{212(1)} - \left\langle {}_rB^{3AHM}_{212}\right\rangle, & \left(\mathrm{v}^{(1)} + \mathrm{v}^{(I)}\right) l_1 < y_1 < l_1 \end{cases}, \tag{42} $$

Table 1
Material properties of layer 1 (Titanium Ti6Al4V [67]) and layer 2 (Ceramic AD-96 [68]).

	E [GPa]	ν
Titanium Ti6A14V	110.3	0.30
Ceramic AD-96	303.0	0.21

Table 2
Effective coefficients for different values of the interface parameters K_n and K_t with volume fraction of layer 2 equal 0.5 and interlayer thickness $t^{(I)} = 10^{-3}$mm.

Models	$K_n = K_t$	C^*_{11}	C^*_{12}	C^*_{23}	C^*_{33}	C^*_{66}
(a) FEM	10^{-3}	0.001000	0.000358	52.160375	219.381185	0.001000
	10	9.547914	3.413901	53.380907	220.601723	8.630479
	10^3	174.330122	62.332545	74.447787	241.669143	59.277656
	10^{12}	211.137193	75.493084	79.190981	246.495981	63.012861
(b) 3AHM	10^{-3}	0.001000	0.000358	52.159220	219.380869	0.001000
	10	9.547786	3.413802	53.379696	220.601351	8.630354
	10^3	174.327578	62.330664	74.445609	241.667806	59.276474
	10^{12}	211.134069	75.490791	79.188582	246.494431	63.011578
(c) 2AHM	10^{-3}	0.001000	0.000358	52.197048	219.502896	0.001000
	10	9.547786	3.413802	53.417522	220.723370	8.630354
	10^3	174.327578	62.330664	74.483191	241.789039	59.276474
	10^{12}	211.134069	75.490791	79.188582	246.494431	63.011578
Difference	$K_n = K_t$	ΔC^*_{11}	ΔC^*_{12}	ΔC^*_{23}	ΔC^*_{33}	ΔC^*_{66}
$\Delta_{ac} = \frac{\lvert(a)-(c)\rvert x100\%}{(a)}$	10^{-3}	0.000000	0.000000	0.070308	0.055479	0.000000
	10	0.001341	0.002900	0.068592	0.055143	0.001448
	10^3	0.001459	0.003018	0.047555	0.049612	0.001994
	10^{12}	0.001480	0.003037	0.003029	0.000629	0.002036
$\Delta_{bc} = \frac{\lvert(b)-(c)\rvert x100\%}{(b)}$	10^{-3}	0.000000	0.000000	0.072524	0.055623	0.000000
	10	0.000000	0.000000	0.070862	0.055312	0.000000
	10^3	0.000000	0.000000	0.050482	0.050165	0.000000
	10^{12}	0.000000	0.000000	0.000000	0.000000	0.000000

where

$$ {}_rB^{3AHM}_{212(s)} = \frac{{}_rA^{3AHM}_{212}}{C^{(s)}_{1212}} - 1, s = 1, 2, 3,\ {}_rA^{3AHM}_{212} = \frac{C^{(1)}_{1212}{}_rC^{(I)}_{1212}C^{(2)}_{1212}}{v^{(2)}C^{(1)}_{1212}{}_rC^{(I)}_{1212} + v^{(I)}C^{(1)}_{1212}C^{(2)}_{1212} + v^{(1)}{}_rC^{(I)}_{1212}C^{(2)}_{1212}}, $$

$$ \left\langle {}_rB^{3AHM}_{212}\right\rangle = \frac{\left(v^{(1)}\right)^2 l_1{}_rB^{3AHM}_{212(1)}}{2} + \frac{\left(v^{(I)}\right)^2 l_1{}_rB^{3AHM}_{212(2)}}{2} + \frac{\left(v^{(2)}\right)^2 l_1{}_rB^{3AHM}_{212(3)}}{2} + \left(v^{(1)}v^{(I)} + v^{(1)}v^{(2)}\right) l_1{}_rB^{3AHM}_{212(1)} + v^{(I)}v^{(2)} l_1{}_rB^{3AHM}_{212(2)}. $$

The effective coefficients are calculated using the formula: $C^*_{ijkl} = \langle C_{ijkl} + C_{ijrs}\,\partial N^{3AHM}_{rkl}/\partial y_s\rangle$, with perfect conditions ($K_n = K_t = \infty$) at the interface. The effective moduli are as follows,

$$ C^{*3AHM}_{1111} = \sum_{r=1}^{N}\theta_r\left\langle\frac{1}{C_{1111}}\right\rangle^{-1}_{Y_r}, C^{*3AHM}_{1122} = C^{*3AHM}_{1133} = \sum_{r=1}^{N}\theta_r\left\langle\frac{1}{C_{1111}}\right\rangle^{-1}_{Y_r}\left\langle\frac{C_{1122}}{C_{1111}}\right\rangle_{Y_r}, $$

$$ C^{*3AHM}_{2222} = C^{*3AHM}_{3333} = \sum_{r=1}^{N}\theta_r\left(\langle C_{1111}\rangle_{Y_r} + \left\langle\frac{1}{C_{1111}}\right\rangle^{-1}_{Y_r}\left\langle\frac{C_{1122}}{C_{1111}}\right\rangle^{2}_{Y_r} - \left\langle\frac{(C_{1122})^2}{C_{1111}}\right\rangle_{Y_r}\right), $$

$$ C^{*3AHM}_{2233} = \sum_{r=1}^{N}\theta_r\left(\langle C_{1122}\rangle_{Y_r} + \left\langle\frac{1}{C_{1111}}\right\rangle^{-1}_{Y_r}\left\langle\frac{C_{1122}}{C_{1111}}\right\rangle^{2}_{Y_r} - \left\langle\frac{(C_{1122})^2}{C_{1111}}\right\rangle_{Y_r}\right), $$

$$ C^{*3AHM}_{1212} = C^{*3AHM}_{1313} = \sum_{r=1}^{N}\theta_r\left\langle\frac{1}{C_{1111}}\right\rangle^{-1}_{Y_r},\ C^{*3AHM}_{2323} = \frac{1}{2}\left[C^{*3AHM}_{2222} - C^{*3AHM}_{2233}\right], \tag{43} $$

where

$$ \left\langle\frac{1}{C_{1111}}\right\rangle^{-1}_{Y_r} = \frac{C^{(1)}_{1111}{}_rC^{(I)}_{1111}C^{(2)}_{1111}}{v^{(2)}C^{(1)}_{1111}{}_rC^{(I)}_{1111} + v^{(I)}C^{(1)}_{1111}C^{(2)}_{1111} + v^{(1)}{}_rC^{(I)}_{1111}C^{(2)}_{1111}}, $$

$$ \left\langle\frac{C_{1122}}{C_{1111}}\right\rangle_{Y_r} = \frac{v^{(2)}C^{(1)}_{1111}{}_rC^{(I)}_{1111}C^{(2)}_{1122} + v^{(I)}C^{(1)}_{1111}C^{(2)}_{1111}{}_rC^{(I)}_{1122} + v^{(1)}{}_rC^{(I)}_{1111}C^{(2)}_{1111}C^{(1)}_{1122}}{C^{(1)}_{1111}{}_rC^{(I)}_{1111}C^{(2)}_{1111}}, $$

Table 3
Behavior of the effective coefficients for 2-interface-partition case.

	$K_n^1 = K_t^1 = 10^{-3}$ and $K_n^2 = K_t^2 = 10^{12}$					
Models	θ_1	C_{11}^*	C_{12}^*	C_{23}^*	C_{33}^*	C_{66}^*
(d) FEM	0.0	211.137193	75.493084	79.190981	246.495981	63.012861
	0.2	168.909955	60.394539	73.784860	241.073021	50.410489
	0.4	126.682716	45.295994	68.378739	235.650062	37.808117
	0.6	84.455477	30.197448	62.972618	230.227103	25.205744
	0.8	42.228239	15.098903	57.566497	224.804144	12.603372
	1.0	0.001000	0.000358	52.160375	219.381185	0.001000
(e) 3AHM	0.0	211.134069	75.490791	79.188582	246.494431	63.011578
	0.2	168.907455	60.392704	73.782710	241.071718	50.409463
	0.4	126.680842	45.294618	68.376837	235.649006	37.807347
	0.6	84.454228	30.196531	62.970965	230.226294	25.205231
	0.8	42.227614	15.098444	57.565092	224.803581	12.603116
	1.0	0.001000	0.000358	52.159220	219.380869	0.001000
(f) 2AHM	0.0	211.134069	75.490791	79.188582	246.494431	63.011578
	0.2	168.907455	60.392704	73.790275	241.096124	50.409463
	0.4	126.680842	45.294618	68.391969	235.697817	37.807347
	0.6	84.454228	30.196531	62.993662	230.299510	25.205231
	0.8	42.227614	15.098444	57.595355	224.901203	12.603116
	1.0	0.001000	0.000358	52.197048	219.502896	0.001000
Difference	θ_1	ΔC_{11}^*	ΔC_{12}^*	ΔC_{23}^*	ΔC_{33}^*	ΔC_{66}^*
$\Delta_{df} = \frac{\lvert(d)-(f)\rvert x100\%}{(d)}$	0.0	0.001480	0.003037	0.003029	0.000629	0.002036
	0.2	0.001480	0.003038	0.007339	0.009583	0.002035
	0.4	0.001479	0.003038	0.019348	0.020265	0.002037
	0.6	0.001479	0.003037	0.033418	0.031450	0.002035
	0.8	0.001480	0.003040	0.050130	0.043175	0.002031
	1.0	0.000000	0.000000	0.070308	0.055479	0.000000
$\Delta_{ef} = \frac{\lvert(e)-(f)\rvert x100\%}{(e)}$	0.0	0.000000	0.000000	0.000000	0.000000	0.000000
	0.2	0.000000	0.000000	0.010253	0.010124	0.000000
	0.4	0.000000	0.000000	0.022130	0.020713	0.000000
	0.6	0.000000	0.000000	0.036044	0.031802	0.000000
	0.8	0.000000	0.000000	0.052572	0.043425	0.000000
	1.0	0.000000	0.000000	0.072524	0.055623	0.000000

$$\left\langle \frac{(C_{1122})^2}{C_{1111}} \right\rangle_{Y_r} = \frac{\mathrm{v}^{(2)} C_{1111}^{(1)} {}_rC_{1111}^{(I)} \left(C_{1122}^{(2)}\right)^2 + \mathrm{v}^{(I)} C_{1111}^{(1)} C_{1111}^{(2)} \left({}_rC_{1122}^{(I)}\right)^2 + \mathrm{v}^{(1)} {}_rC_{1111}^{(I)} C_{1111}^{(2)} \left(C_{1122}^{(1)}\right)^2}{C_{1111}^{(1)} {}_rC_{1111}^{(I)} C_{1111}^{(2)}},$$

$$\left\langle \frac{1}{C_{1212}} \right\rangle_{Y_r}^{-1} = \frac{C_{1212}^{(1)} {}_rC_{1212}^{(I)} C_{1212}^{(2)}}{\mathrm{v}^{(2)} C_{1212}^{(1)} {}_rC_{1212}^{(I)} + \mathrm{v}^{(I)} C_{1212}^{(1)} C_{1212}^{(2)} + \mathrm{v}^{(1)} {}_rC_{1212}^{(I)} C_{1212}^{(2)}},$$

$$\left\langle C_{ijkl} \right\rangle_{Y_r} = \mathrm{v}^{(1)} C_{ijkl}^{(1)} + \mathrm{v}^{(I)} {}_rC_{ijkl}^{(I)} + \mathrm{v}^{(2)} C_{ijkl}^{(2)}.$$

3.3. Interface models

Analytical expressions for the elastic interlayer representing the interlayer properties can be written based on the constituent properties and geometry. Thus, the two-phase model with imperfect interface conditions (spring type) is modeled as a three-phase material with perfect conditions. The coefficients C_{2222}^* and C_{2233}^* depend on the coefficients C_{1111}^* and C_{1122}^*, so only C_{1111}^*, C_{1122}^* and C_{1212}^* are involved in the derivation of the properties of the interface. Hence, by equaling the effective coefficients C_{1111}^*, C_{1122}^*, and C_{1212}^* from Eqs. (36) and (43), the interface modulus for the r-interface-partition can be written as:

$$\begin{aligned}
{}_rC_{1111}^{(I)} &= \frac{\mathrm{v}^{(I)} t^{(I)} {}_rK_n C_{1111}^{(1)} C_{1111}^{(2)}}{\left[(1-\gamma-\mathrm{v}^{(2)})C_{1111}^{(1)} + (\gamma-\mathrm{v}^{(1)})C_{1111}^{(2)}\right] t^{(I)} {}_rK_n + \mathrm{v}^{(I)} C_{1111}^{(1)} C_{1111}^{(2)}}, \\
{}_rC_{1122}^{(I)} &= \frac{\left(\mathrm{v}^{(2)} C_{1111}^{(1)} {}_rC_{1111}^{(I)} + \mathrm{v}^{(I)} C_{1111}^{(1)} C_{1111}^{(2)} + \mathrm{v}^{(1)} {}_rC_{1111}^{(I)} C_{1111}^{(2)}\right)\left[(1-\gamma)C_{1111}^{(1)} C_{1122}^{(2)} + \gamma C_{1111}^{(2)} C_{1122}^{(1)}\right] t^{(I)} {}_rK_n}{\mathrm{v}^{(I)} C_{1111}^{(1)} C_{1111}^{(2)} \left\{\left[(1-\gamma)C_{1111}^{(1)} + \gamma C_{1111}^{(2)}\right] t^{(I)} {}_rK_n + \mathrm{v}^{(I)} C_{1111}^{(1)} C_{1111}^{(2)}\right\}} - \\
&\quad - \frac{\mathrm{v}^{(2)} {}_rC_{1111}^{(I)} C_{1122}^{(2)}}{\mathrm{v}^{(I)} C_{1111}^{(2)}} - \frac{\mathrm{v}^{(1)} {}_rC_{1111}^{(I)} C_{1122}^{(1)}}{\mathrm{v}^{(I)} C_{1111}^{(1)}}, \\
{}_rC_{1212}^{(I)} &= \frac{\mathrm{v}^{(I)} t^{(I)} {}_rK_t C_{1212}^{(1)} C_{1212}^{(2)}}{\left[\left(1-\gamma-\mathrm{v}^{(2)}\right)C_{1212}^{(1)} + \left(\gamma-\mathrm{v}^{(1)}\right)C_{1212}^{(2)}\right] t^{(I)} {}_rK_t + \mathrm{v}^{(I)} C_{1212}^{(1)} C_{1212}^{(2)}},
\end{aligned} \tag{44}$$

Table 4
Behavior of the effective coefficients for 3-interface-partition case.

	$K_n^1 = K_t^1 = 10$, $K_n^2 = K_t^2 = 10^{-3}$ and $K_n^3 = K_t^3 = 10^{12}$					
Models	θ_2	C_{11}^*	C_{12}^*	C_{23}^*	C_{33}^*	C_{66}^*
(g) FEM	0.0	59.945234	21.433697	59.833425	227.075287	22.226074
	0.2	47.956387	17.147029	58.298815	225.536467	17.781059
	0.4	35.967540	12.860361	56.764205	223.997646	13.336045
	0.6	23.978694	8.573693	55.229595	222.458826	8.891030
	0.8	11.989847	4.287025	53.694985	220.920005	4.446015
	1.0	0.001000	0.000358	52.160375	219.381185	0.001000
(h) 3AHM	0.0	59.944357	21.433049	59.831917	227.074621	22.225660
	0.2	47.955685	17.146511	58.297378	225.535871	17.780728
	0.4	35.967014	12.859973	56.762838	223.997120	13.335796
	0.6	23.978343	8.573434	55.228299	222.458370	8.890864
	0.8	11.989671	4.286896	53.693759	220.919620	4.445932
	1.0	0.001000	0.000358	52.159220	219.380869	0.001000
(i) 2AHM	0.0	59.944357	21.433049	59.860287	227.166135	22.225660
	0.2	47.955685	17.146511	58.327639	225.633487	17.780728
	0.4	35.967014	12.859973	56.794991	224.100839	13.335796
	0.6	23.978343	8.573434	55.262343	222.568192	8.890864
	0.8	11.989671	4.286896	53.729696	221.035544	4.445932
	1.0	0.001000	0.000358	52.197048	219.502896	0.001000
Difference	θ_2	ΔC_{11}^*	ΔC_{12}^*	ΔC_{23}^*	ΔC_{33}^*	ΔC_{66}^*
$\Delta_{gi} = \frac{\lvert(g)-(i)\rvert x100\%}{(g)}$	0.0	0.001463	0.003023	0.044895	0.040008	0.001863
	0.2	0.001464	0.003021	0.049442	0.043017	0.001862
	0.4	0.001462	0.003017	0.054235	0.046069	0.001867
	0.6	0.001464	0.003021	0.059294	0.049162	0.001867
	0.8	0.001468	0.003009	0.064645	0.052299	0.001867
	1.0	0.000000	0.000000	0.070308	0.055479	0.000000
$\Delta_{hi} = \frac{\lvert(h)-(i)\rvert x100\%}{(h)}$	0.0	0.000000	0.000000	0.047416	0.040301	0.000000
	0.2	0.000000	0.000000	0.051908	0.043282	0.000000
	0.4	0.000000	0.000000	0.056644	0.046304	0.000000
	0.6	0.000000	0.000000	0.061642	0.049367	0.000000
	0.8	0.000000	0.000000	0.066930	0.052473	0.000000
	1.0	0.000000	0.000000	0.072524	0.055623	0.000000

where $t^{(I)}$ is the interlayer thickness. In fact, Eqs. (44) comprise the interlayer properties, which are equivalent to the effect of non-uniform imperfect adhesion.

3.4. FEM: three-layer elastic composite

Based on the RVE concept combined with FEM, and considering interface effects, it can be calculated the effective properties of the elastic composites with interface effects. The interface properties of the FEM three-layer model are calculated using the interface model defined in Eq. (44).

The RVE is an important concept in studies of the mechanical responses of heterogeneous materials, where it constitutes the smallest material volume element of the composite, thereby providing a highly accurate model for representing the material's response. The effective stresses and strains of the macroscopically homogeneous medium are derived by averaging the stresses and strains tensor over the RVE:

$$\bar{\sigma}_{ij} = \sum_{r=1}^{N} \theta_r \langle \sigma_{ij}^r \rangle_{Y_r} = \sum_{r=1}^{N} \frac{\theta_r}{|Y_r|} \int_V {}_r\sigma_{ij}\, dY, \bar{\varepsilon}_{ij} = \sum_{r=1}^{N} \theta_r \langle \varepsilon_{ij}^r \rangle_{Y_r} = \sum_{r=1}^{N} \frac{\theta_r}{|Y_r|} \int_V {}_r\varepsilon_{ij}\, dY, \tag{45}$$

where $|Y_r|$ is the unit cell volume of the unit cell portion Y_r.

By discretizing Eq. (45), the average values can be calculated as:

$$\bar{\sigma}_{ij} = \sum_{r=1}^{N} \frac{\theta_r}{|Y_r|} \sum_{m=1}^{nel} {}_r\sigma_{ij}^{(m)} Y_r^{(m)}, \quad \bar{\varepsilon}_{ij} = \sum_{r=1}^{N} \frac{\theta_r}{|Y_r|} \sum_{m=1}^{nel} {}_r\varepsilon_{ij}^{(m)} Y_r^{(m)}, \tag{46}$$

where *nel* is the number of finite elements, $Y_r^{(m)}$ is the volume of the mth finite element, and ${}_r\sigma_{ij}^{(m)}$ and ${}_r\varepsilon_{ij}^{(m)}$ are the respective stress and strain tensors evaluated in the mth finite element.

Under a uniform loading, the stress and strain state is uniform in a homogeneous material, but this is not the case in a layered composite. However, all of the RVEs are identical so they exhibit identical stress and strain fields. Thus, each RVE in the layered composite has the same deformation mode, and there is no separation or overlap between the neighboring RVEs. These periodic boundary conditions are used to determine the appropriate displacement constraints at the boundary

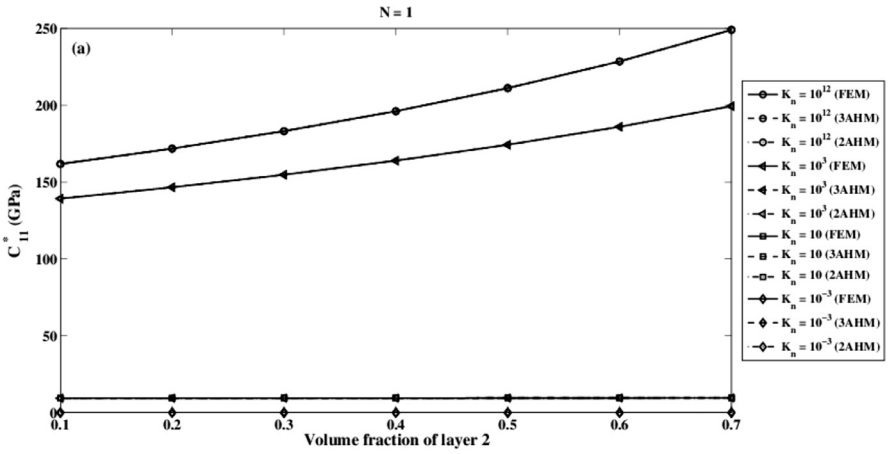

(a)

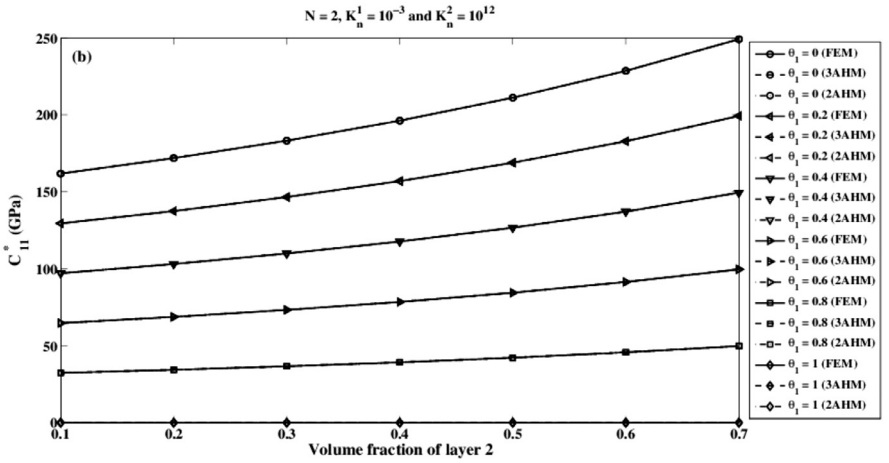

(b)

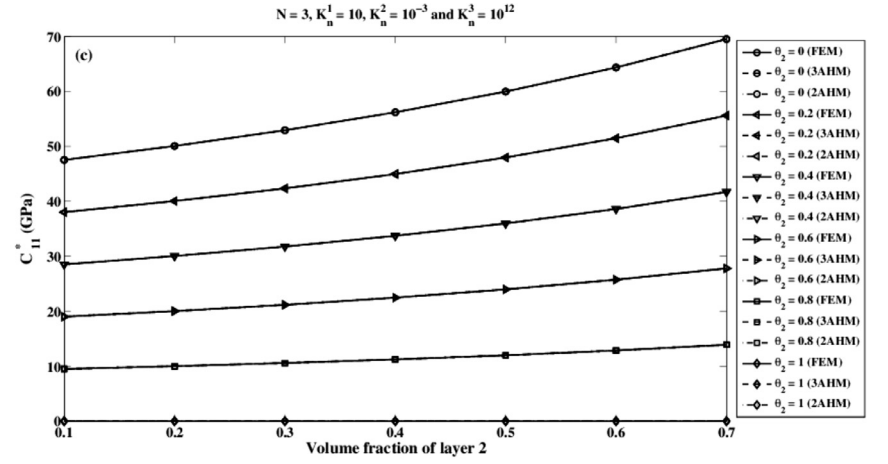

(c)

Fig. 3. Evolution of elastic property C^*_{11} as a function of the volume fraction of layer 2: (a) uniform imperfect interface ($N = 1$), (b) two-interface partition ($N = 2$, $\theta_2 = 1 - \theta_1$), and (c) three-interface partition ($N = 3$, $\theta_1 = 0.75 \bullet (1 - \theta_2)$, $\theta_3 = 0.25 \bullet (1 - \theta_2)$).

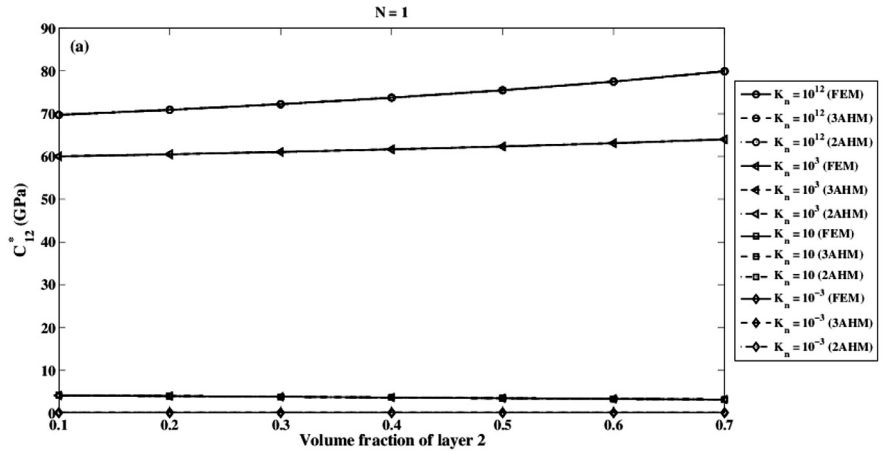

(a)

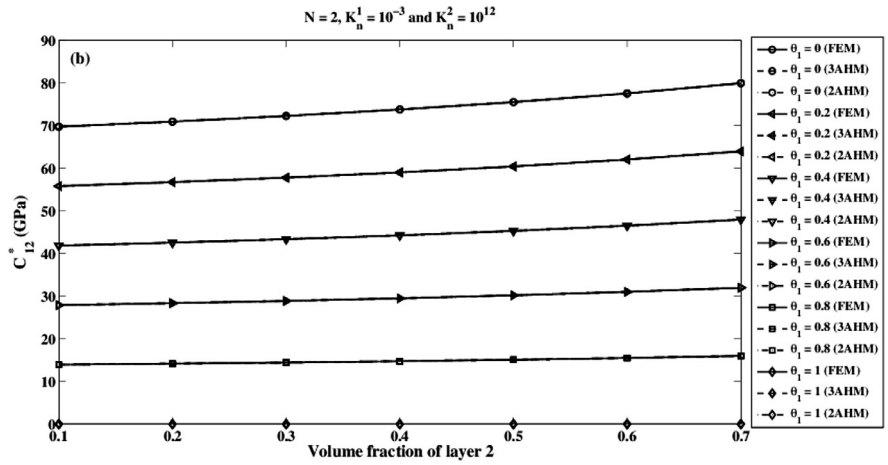

(b)

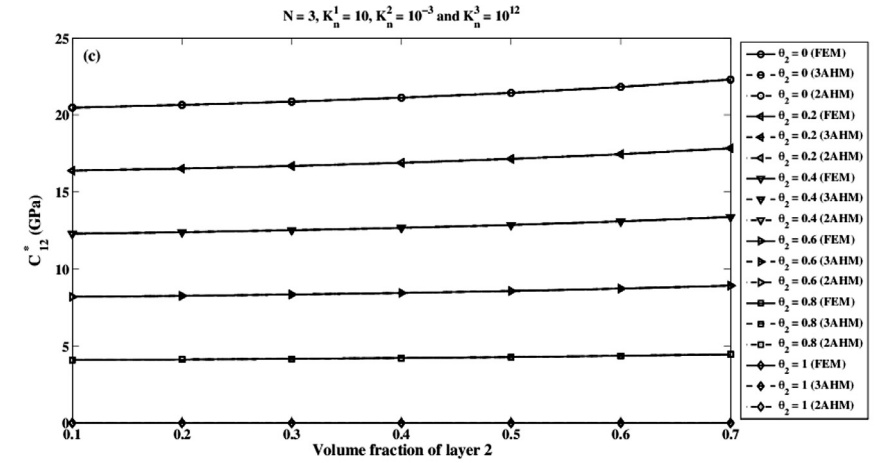

(c)

Fig. 4. Evolution of elastic property C^*_{12} as a function of the volume fraction of layer 2: (a) uniform imperfect interface ($N = 1$), (b) two-interface partition ($N = 2$, $\theta_2 = 1 - \theta_1$), and (c) three-interface partition ($N = 3$, $\theta_1 = 0.75 \bullet (1 - \theta_2)$, $\theta_3 = 0.25 \bullet (1 - \theta_2)$).

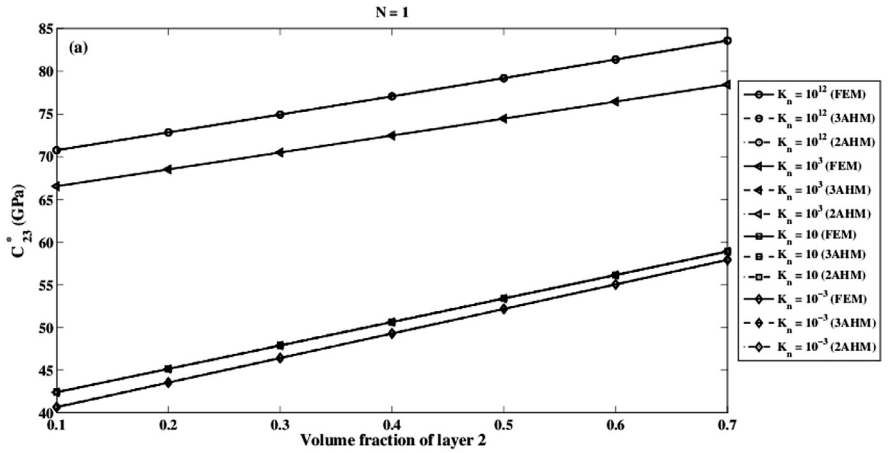

(a)

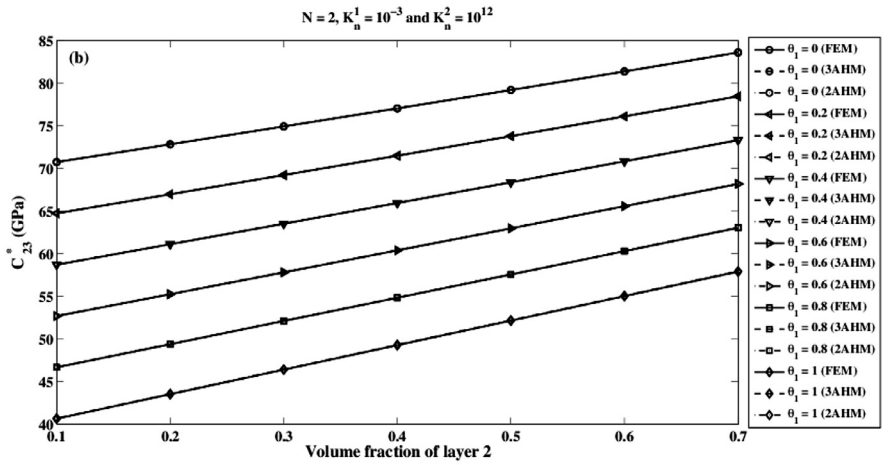

(b)

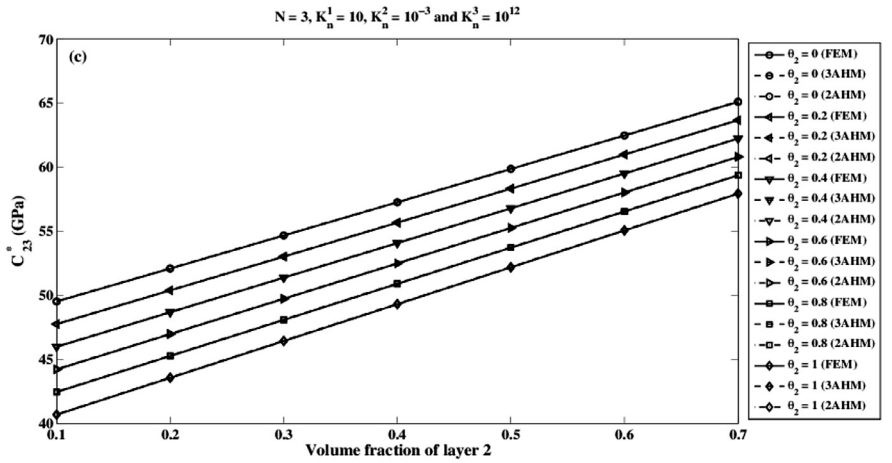

(c)

Fig. 5. Evolution of elastic property C^*_{23} as a function of the volume fraction of layer 2: (a) uniform imperfect interface ($N = 1$), (b) two-interface partition ($N = 2$, $\theta_2 = 1 - \theta_1$), and (c) three-interface partition ($N = 3$, $\theta_1 = 0.75 \bullet (1 - \theta_2)$, $\theta_3 = 0.25 \bullet (1 - \theta_2)$).

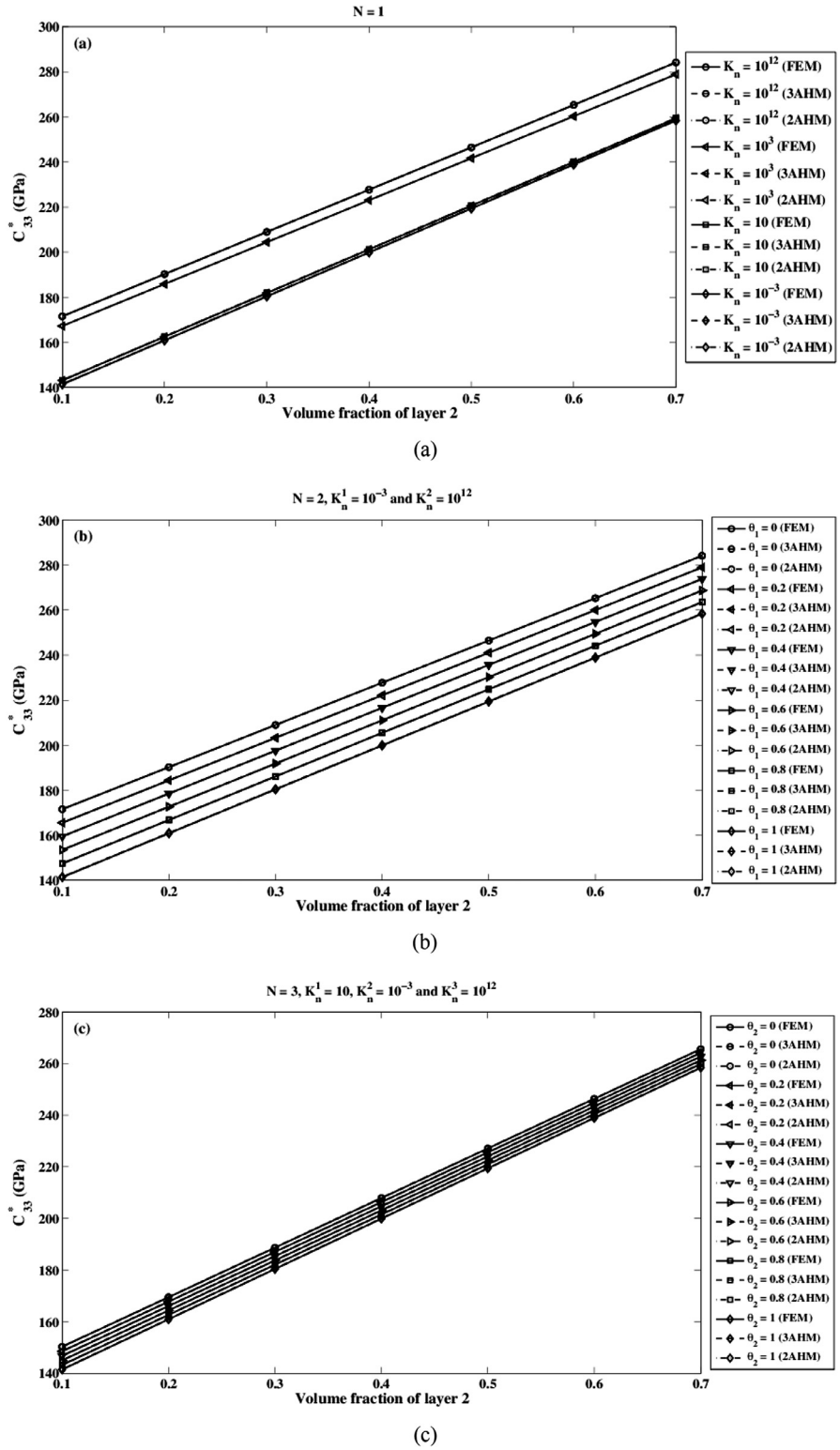

Fig. 6. Evolution of elastic property C^*_{33} as a function of the volume fraction of layer 2: (a) uniform imperfect interface ($N = 1$), (b) two-interface partition ($N = 2$, $\theta_2 = 1 - \theta_1$), and (c) three-interface partition ($N = 3$, $\theta_1 = 0.75 \bullet (1 - \theta_2)$, $\theta_3 = 0.25 \bullet (1 - \theta_2)$).

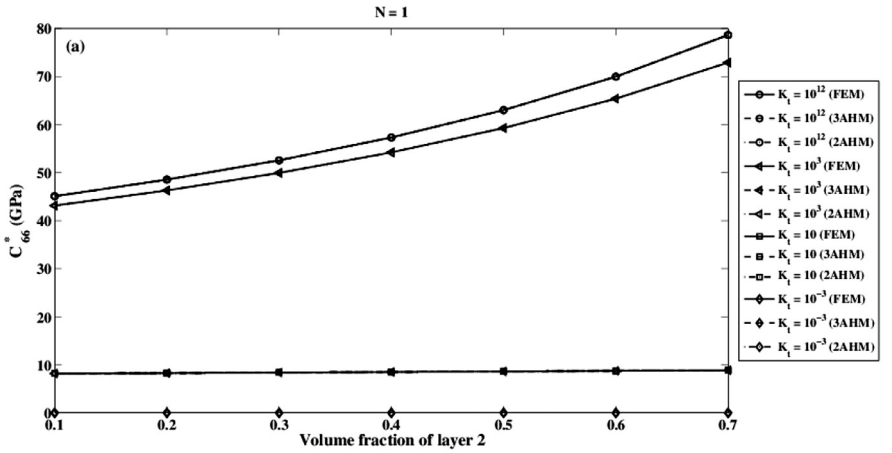

(a)

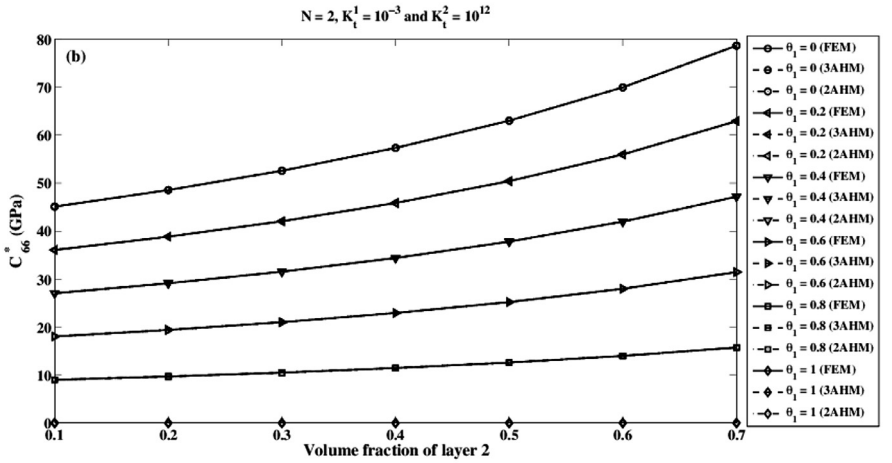

(b)

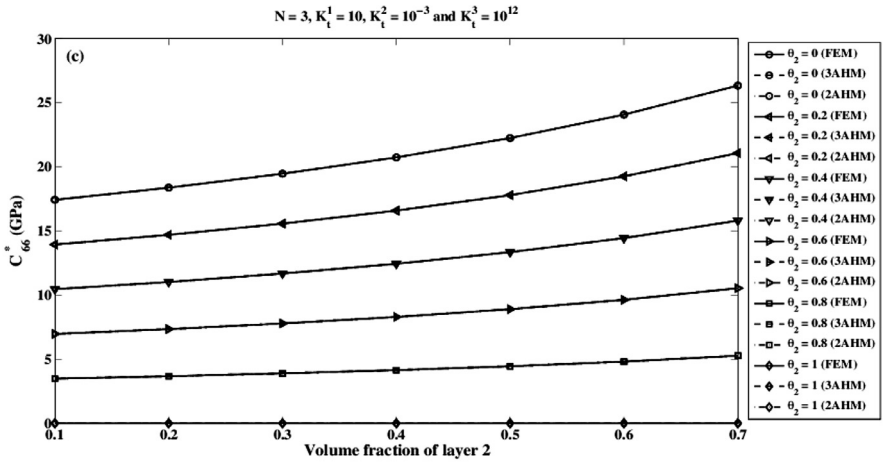

(c)

Fig. 7. Evolution of elastic property C^*_{66} as a function of the volume fraction of layer 2: (a) uniform imperfect interface ($N = 1$), (b) two-interface-partition ($N = 2$, $\theta_2 = 1 - \theta_1$), and (c) three-interface-partition ($N = 3$, $\theta_1 = 0.75 \cdot (1 - \theta_2)$, $\theta_3 = 0.25 \cdot (1 - \theta_2)$).

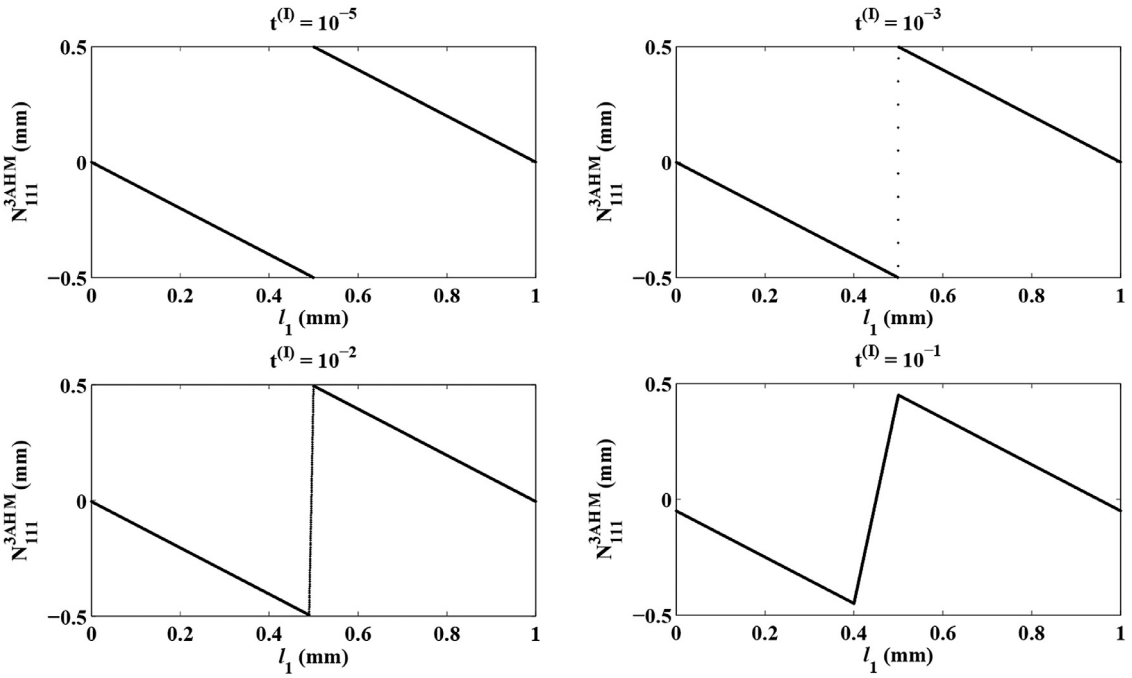

Fig. 8. Uniform imperfect interface local function N_{111}^{3AHM} for different values of the interlayer thickness $t^{(I)}$ and interface parameter $K_n = 10^{-3}$ where the volume fraction of layer 2 is 0.5.

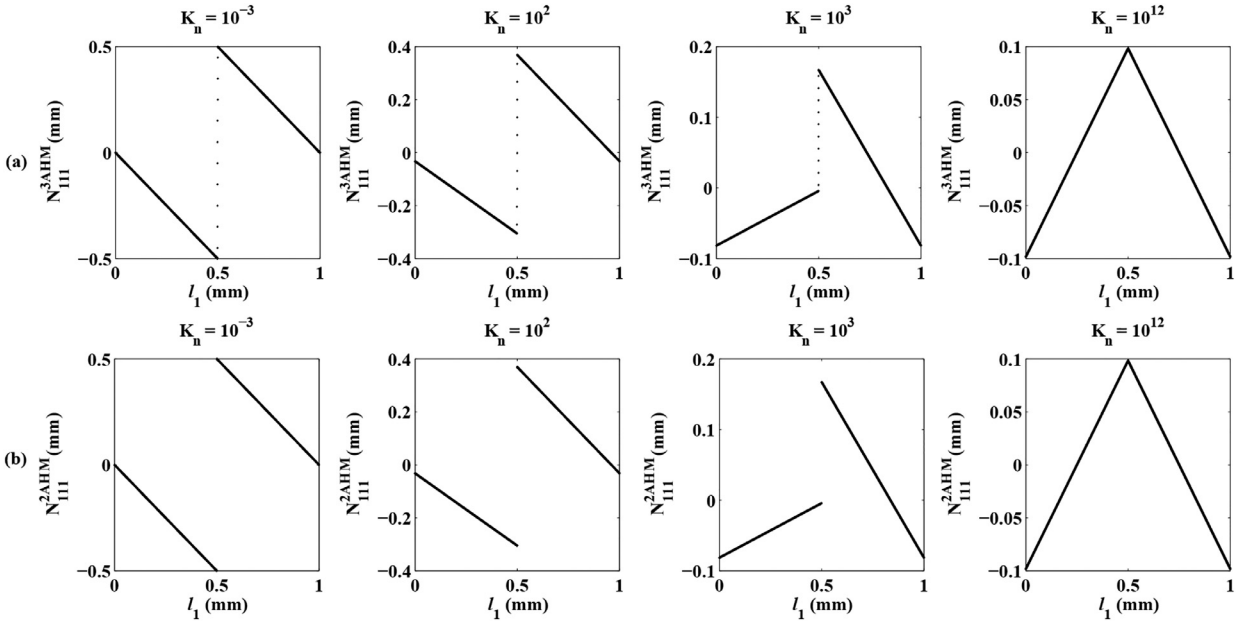

Fig. 9. Uniform imperfect interface local function N_{111} for different values of the interface parameter K_n and interlayer thickness $t^{(I)} = 10^{-3}$ where the volume fraction of layer 2 is 0.5: (a) AHM three-phase perfect, and (b) AHM two-phase spring.

of the RVE by FEM using ABAQUS™ combined with the PYTHON language. In addition, the three phases of the FEM–RVE model are modeled by solid elements with a linear interpolation shape function.

4. Results

In order to show the effects of non-uniform imperfect adhesion on the effective properties, some analytical and numerical investigations were performed. Thus, a mesh sensitivity study was conducted by considering three mesh densities

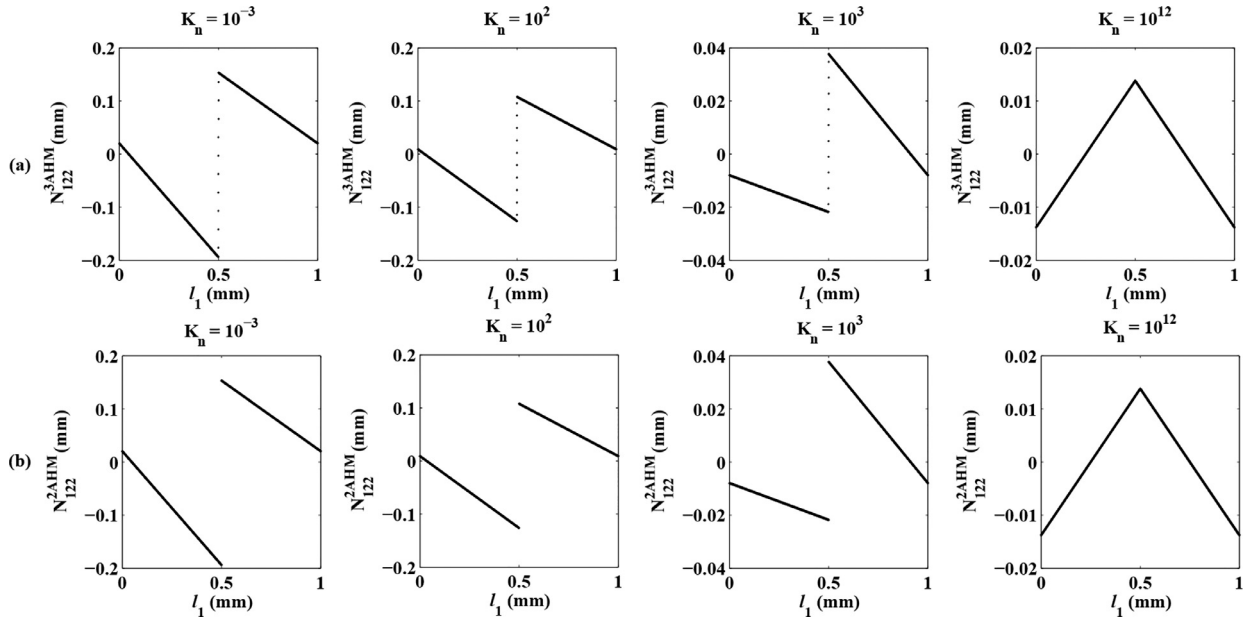

Fig. 10. Uniform imperfect interface local function N_{122} for different values of the interface parameter K_n and interlayer thickness $t^{(I)} = 10^{-3}$ where the volume fraction of layer 2 is 0.5: (a) AHM three-phase perfect, and (b) AHM two-phase spring.

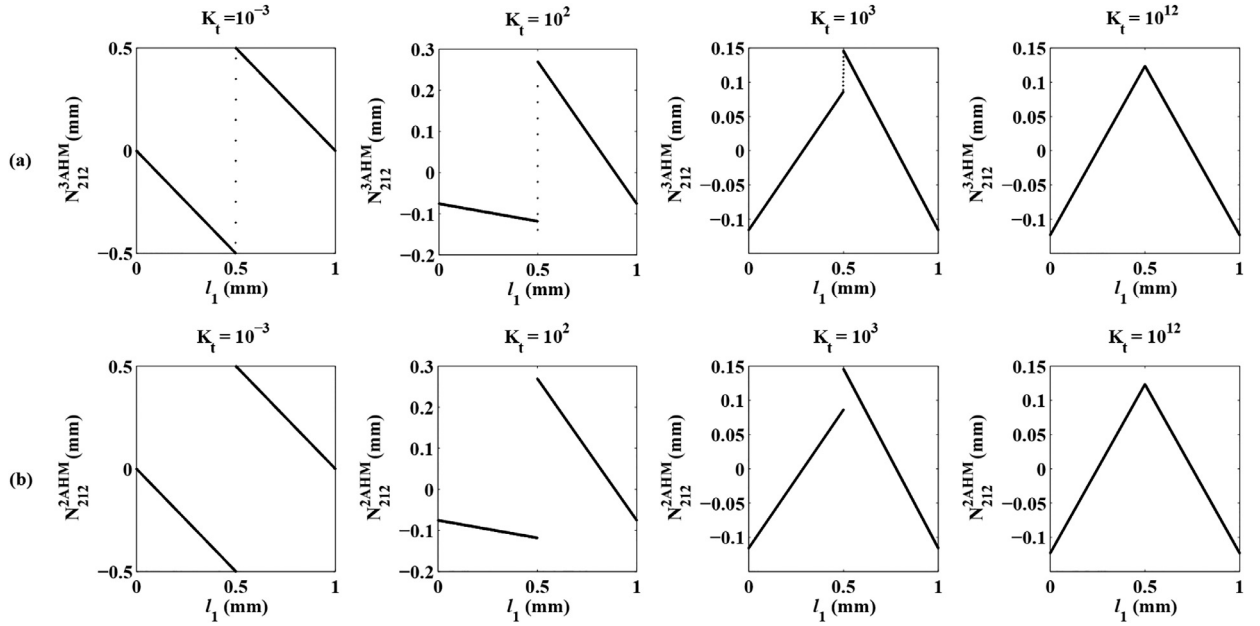

Fig. 11. Uniform imperfect interface local function N_{212} for different values of the interface parameter K_t and interlayer thickness $t^{(I)} = 10^{-3}$ where the volume fraction of layer 2 is 0.5: (a) AHM three-phase perfect, and (b) AHM two-phase spring.

for the unit cell, which was solved by FEM. The results demonstrated that a mesh density with 4000 finite elements was sufficient to obtain consistent numerical results. Therefore, the results obtained using this meshed RVE were compared with the analytical solutions.

The material properties reported in previous studies are shown in Table 1 [67,68]. In the analyses, the interface volume fraction ($v^{(I)}$) and length (l_1) of the unit cell in the y_1 direction were assumed to be equal to 10^{-3} and 1 mm, respectively. Thus, as shown in Table 2, the effective coefficients for uniform imperfection were calculated for different values of the interface parameters K_n and K_t with K_n $v^{(2)} = 0.5$. The calculated relative differences between the three-layer and two-layer models are shown, where the three-layer model achieved excellent convergence. The effective coefficients with the highest differences were C_{23}^{*} and C_{33}^{*} when K_n was equal to 10^{-3} GPa/mm, which were smaller than 0.073% and 0.056%, respectively.

These differences can be explained by the fact that interface stiffness K_n is present in all terms of the effective coefficients C^*_{23} and C^*_{33} (see Eq. (43)). However, for the two-layer model, only the second term depends on the interface stiffness K_n (see Eq. (36)).

First, the two-interface partition was studied for different values of the parameter θ_1 (degree imperfection) with $v^{(2)} = 0.5$ (Table 3), where we simulated the separation of the interface starting from an extreme. In this case, the differences in the coefficients C^*_{11}, C^*_{12}, and C^*_{66} remained approximately equal to the percentage difference in the perfect bonding case as the degree of imperfection θ_1 increased. The percentage differences for the coefficients C^*_{23}, and C^*_{33} increased as the degree of imperfection increased.

As shown in Table 4, the coefficients were calculated for different degrees of imperfection θ_2 for the three-interface partition by simulating the separation of the interface starting from the inside. The differences in the coefficients C^*_{11}, C^*_{12}, and C^*_{66} were similar to the results for the two-interface partition case. However, the differences in the coefficients C^*_{23} and C^*_{33} were significantly higher than those for the two-interface partition case for degree of imperfection values of $\theta_2 = 0$, 0.2 and 0.4.

Figs. 3–7 show the effective coefficients as a function of $v^{(2)}$ for different imperfect interface cases, which were obtained by simulating a delamination process. In each plot, the three-layer results are compared to the two-layer imperfect interface results, where it is clear that the plots are numerically indistinguishable. The effective coefficients C^*_{11}, C^*_{12}, and C^*_{66} with K_n equal to 10^{12} GPa/mm for $\theta_1 = 0$ and $\theta_2 = 0$ increased with $v^{(2)}$, where they remained close to zero for $\theta_1 = 1$ and $\theta_2 = 1$. However, the values of C^*_{23} and C^*_{33} differed.

The uniform imperfect interface local function N^{3AHM}_{111} for different values of the interlayer thickness $t^{(I)}$ is shown in Fig. 8. Clearly, as the interlayer thickness increased, the behavior of the third branch differed in the plots where it changed from discontinuous to continuous. The same conclusion applied to the other non-zero local functions. This change can be attributed to the increase in the thickness of the interlayer.

The changes in the three-layer and two-layer uniform imperfect interface local functions with an interlayer thickness of $t^{(I)} = 10^{-3}$ and different values for the interface parameters K_n and K_t are shown in Figs. 9–11, which indicate that with complete separation of the layers, the local functions decreased as the length l_1 increased. Different behaviors were found in terms of the monotonicity of the local functions for perfect bonding, where they increased first and then decreased. In addition, the values of the local functions for imperfect bonding were larger than those of the local functions for perfect bonding.

5. Conclusions

In this study, we employed two approaches to model non-uniform imperfect adhesion in layered composites, *i.e.*, at the macro-scale level. Using the results obtained by the two-layer model with non-uniform imperfect interface conditions (spring type) and the three-layer material with perfect conditions, an interface model was derived to calculate the interlayer properties in the case of three-layer composites. It was shown that the results obtained by the three-layer model provided an excellent approximation to the results using the two-layer spring problem.

In general, based on the effective coefficients for different imperfect adhesion cases investigated by AHM, it is possible to conclude that the effective properties increased as $v^{(2)}$ increased for $\theta_1 = 0$ and $\theta_2 = 0$. For $\theta_1 = 1$ and $\theta_2 = 1$, the effective coefficients remained close to zero as $v^{(2)}$ increased. However, the coefficients C^*_{23} and C^*_{33} always increased as $v^{(2)}$ increased. In addition, the FEM–RVE results confirmed these remarks. The results obtained using uniform imperfect adhesion local functions for complete separation were higher than those for perfect bonding. For two- and three-interface partitions, the imperfection increased as the degree of imperfection values θ_1 and θ_2 increased when we simulated a delamination or debonding process. Therefore, the proposed approaches can be used to study the separation along the interfaces of the layers, *i.e.*, delamination or debonding.

The interlayer had no volume in the two-layer imperfect model. However, the interlayer had a volume in the three-layer model, where it produced changes in the overall thickness of the laminate. This difference may be relevant mainly for problems that involve bending or twisting. For example, Takahashi [27] estimated the strength of ceramic–metal joints with different interlayer thicknesses and showed that the bending strength changed. Therefore, in future research, it will be investigated the influence of the interlayer thickness in problems that involve bending or twisting.

Finally, the analytical and computational models proposed in the present study may facilitate the design of layered composites by predicting their effective properties considering non-uniform imperfect adhesion between layers (e.g., debonding). This is very important for the development of different types of structures used in fighter aircraft, such as layered composite shields, which must have high ballistic resistance. In addition, the proposed approaches can be extended to other composite structures used in the automotive, aeronautical, and other industries, mainly to support design for certification processes.

Acknowledgments

The authors thank Coordination for the Improvement of the Higher Level Personnel (CAPES/PNPD) and National Council for Scientific and Technological Development (CNPq process numbers: 401170/2014-4 and 310094/2015-1). The authors also thank Prof. Marcelo Leite Ribeiro (University of São Paulo) for providing ABAQUS™ software.

References

[1] G.R. Wooley, D.R. Carver, Stress concentration factors for bonded lap joints, J. Aircraft. 8 (1971) 817–820.

[2] T. Wah, Stress distribution in a bonded anisotropic lap joint, J. Eng. Mater Technol. ASME 95 (1973) 174–181.
[3] I.U. Ojalvo, H.L. Eidinoff, Bond thickness effects upon stresses in single-lap adhesive joints, AIAA J. 16 (1978) 204–211.
[4] F. Delale, F. Erdogan, M.N. Aydinoglu, Stresses in adhesively bonded joints: a closed-form solution, J. Compos. Mater. 15 (1981) 249–271.
[5] D. Chen, S. Cheng, An analysis of adhesive-bonded single-lap joints, J. Appl. Mech. ASME 50 (1983) 109–115.
[6] R.D. Adams, J. Comyn, W.C. Wake, Structural Adhesive Joints in Engineering, Elsevier Applied Science, London and New York, 1984.
[7] A. Higgins, Adhesive bonding of aircraft structures, Int. J. Adhes. Adhes. 20 (2000) 367–376.
[8] H. Sun, N. Pan, Mechanical characterization of the interfaces in laminated composites, Compos. Struct. 74 (2006) 25–29.
[9] G.C. Knollman, Variation of shear modulus through the interfacial bond zone of an adhesive, Int. J. Adhes. Adhes. 5 (1985) 137–141.
[10] V. Safavi-Ardebili, A.N. Sinclair, J.K. Spelt, Experimental investigation of the interphase in an epoxy-aluminum system, J. Adhes. 62 (1997) 93–111.
[11] J.K. Krüeger, W. Possart, R. Bactavachalou, U. Müeller, T. Britz, R. Sanctuary, P. Alnot, Gradient of the mechanical modulus in glass-epoxy-metal joints as measured by Brillouin microscopy, J. Adhes. 80 (2004) 585–599.
[12] J. Chung, M. Munz, H. Sturm, Stiffness variation in the interphase of amine-cured epoxy adjacent to copper microstructures, Surf. Interf. Anal. 39 (2007) 624–633.
[13] P.P. Parlevliet, H.E.N. Bersee, A. Beukers, Residual stresses in thermoplastic composites—A study of the literature—Part II: Experimental techniques, Compos. Part A Appl. Sci. Manuf. 38 (2007) 651–665.
[14] H. Leidheiser Jr., P.D. Deck, Chemistry of the metal-polymer interfacial region, Science 241 (1988) 1176–1181.
[15] K. Davey, An analytical solution for the unidirectional solidification problem, Appl. Math. Model. 17 (1993) 658–663.
[16] M. Benabdi, A.A. Roche, Mechanical properties of thin and thick coatings applied to various substrates. Part I. An elastic analysis of residual stresses within coating materials, J. Adhes. Sci. Technol. 11 (1997) 281–299.
[17] S. Bentadjine, V. Massardier, R. Petiaud, A.A. Roche, Organo-metallic complex characterization formed when liquid epoxy-diamine mixtures are applied onto metallic substrates, Polymer 42 (2001) 6271–6282.
[18] C. Wehlack, W. Possart, Characterization of the epoxy-metal interphase: FTIR-ERAS and spectral calculation for ultra-thin films, Macromol. Symp. 205 (2004) 251–261.
[19] P. Montois, V. Nassiet, J.A. Petit, Y. Bazaiard, Viscosity effect on epoxy–diamine/metal interphases Part I: thermal and thermomechanical behaviour, Int. J. Adhes. Adhes. 26 (2006) 391–399.
[20] P.P. Shi, Imperfect interface effect for nano-composites accounting for fiber section shape under antiplane shear, Appl. Math. Model 43 (2017) 393–408.
[21] P.L. Geiss, M. Schumann, Investigation of the mechanical properties of interphases in adhesively bonded epoxy-aluminum joints by localized micro extensometry, J. Adhes. 88 (2012) 941–955.
[22] R. Massabò, F. Campi, An efficient approach for multilayered beams and wide plates with imperfect interfaces and delamination, Compos. Struct 116 (2014) 311–324.
[23] R. Massabò, F. Campi, Assessment and correction of theories for multilayered plates with imperfect interfaces, Meccanica 50 (2015) 1045–1071.
[24] L. Librescu, R. Schmidt, A general theory of laminated composite shells featuring interlaminar bonding imperfections, Int. J. Solids Struct. 38 (2001) 3355–3375.
[25] R. Massabò, F. Campi, Modeling laminated composites with cohesive interfaces: a homogenization approach, in: Proceedings of the XXI Congress of the Italian Association of Theoretical & Applied Mechanics AIMETA Torino, 2013, pp. 1–10. ISBN 978-88-8239-183-6.
[26] R. Massabò, F. Campi, Delamination damage in laminated shells, in: Proceedings of the 19th International Conference on Composite Materials (ICCM), Montreal, Canada, 2013, pp. 1–10. ISBN 9781629931999.
[27] M. Takahashi, N. Okabe, X. Zhu, K. Kagawa, Strength estimation of ceramic-metal joints with various interlayer thickness, Fatigue Fract. Eng. Mater. Struct. 26 (2003) 391–398.
[28] L.J. Walpole, A coated inclusion in an elastic medium, Math. Proc. Camb. Philos. Soc. 83 (1978) 495–506.
[29] H.L. Duan, X. Yi, Z.P. Huang, J. Wang, A unified scheme for prediction of effective moduli of multiphase composites with interface effects. Part I: theoretical framework, Mech. Mater. 39 (2007) 81–93.
[30] H.L. Duan, X. Yi, Z.P. Huang, J. Wang, A unified scheme for prediction of effective moduli of multiphase composites with interface effects. Part II—Application and scaling laws, Mech. Mater 39 (2007) 94–103.
[31] J.C. López-Realpozo, R. Rodríguez-Ramos, R. Guinovart-Díaz, J. Bravo-Castillero, F.J. Sabina, Transport properties in fibrous elastic rhombic composite with imperfect contact condition, Int. J. Mech. Sci. 53 (2011) 98–107.
[32] R. Rodríguez-Ramos, R. Medeiros, R. Guinovart-Díaz, J. Bravo-Castillero, J.A. Otero, V. Tita, Different approaches for calculating the effective elastic properties in composite materials under imperfect contact adherence, Compos. Struct. 99 (2013) 264–275.
[33] Y. Benveniste, T. Miloh, The effective conductivity of composites with imperfect thermal contact at constituent interfaces, Int. J. Eng. Sci. 24 (1986) 1537–1552.
[34] N.J. Pagano, G.P. Tando, Elastic response of multi-directional coated-fiber composite, Compos. Sci. Technol. 31 (1988) 273–293.
[35] E. Sideridis, The in-plane shear modulus of fiber reinforced composites as defined by the concept of interphase, Compos. Sci. Technol. 31 (1988) 35–53.
[36] R. Rizzoni, F. Lebon, Asymptotic analysis of an adhesive joint with mismatch strain, Eur. J. Mech. A Solids 36 (2012) 1–8.
[37] Y.D. Li, T. Xiong, L. Dong, A new interfacial imperfection coupling model (IICM) and its effect on the facture behavior of a layered multiferroic composite: Anti-plane case, Eur. J. Mech. A Solids 52 (2015) 26–36.
[38] V. Tita, R. Medeiros, F.D. Marques, M.E. Moreno, Effective properties evaluation for smart composite materials with imperfect fiber–matrix adhesion, J. Compos. Mater. 49 (2015) 3683–3701.
[39] R. Rodríguez-Ramos, R. Guinovart-Díaz, J.C. López-Realpozo, J. Bravo-Castillero, F.J. Sabina, F. Lebon, S. Dumont, M. Würkner, H. Berger, U. Gabbert, Characterization of piezoelectric composites with mechanicalelectrical imperfect contacts, J. Compos. Mater. 50 (2016) 1603–1625.
[40] A.K. Mal, S.K. Bose, Dynamic elastic moduli of a suspension of imperfectly bonded spheres, Math. Proc. Camb. Philos. Soc. 76 (1975) 587–600.
[41] Y. Benveniste, The effective mechanical behaviour of composite materials with imperfect constant between the constituents, Mech. Mater. 4 (1985) 197–208.
[42] J. Aboudi, Damage in composites–modeling of imperfect bonding, Compos. Sci. Technol. 28 (1987) 103–128.
[43] J.D. Achenbach, H. Zhu, Effect of interfacial zone on mechanical behavior failure of fiber-reinforced composites, J. Mech. Phys. Solids 37 (1989) 381–393.
[44] N.J. Pagano, G.P. Tandon, Modelling of imperfect bonding in fiber reinforced brittle matrix composites, Mech. Mater. 9 (1990) 49–64.
[45] J. Qu, The effect of slightly weakened interfaces on the overall elastic properties of composite materials, Mech. Mater. 14 (1993) 269–281.
[46] Y. Wu, Z. Ling, Z. Dong, Stress–strain fields and the effectiveness shear properties for three-phase composites with imperfect interface, Int. J. Solids Struct. 37 (2000) 1275–1292.
[47] S. Lenci, G. Menditto, Weak interface in long fibre composites, Int. J. Solids Struct. 37 (2000) 4239–4260.
[48] Z. Hashin, Thin interphase/imperfect interface in conduction, J. Appl. Phys. 89 (2001) 2261–2267.
[49] Z. Hashin, Thin interphase/imperfect interface in elasticity with application to coated fiber composite, J. Mech. Phys. Solids 50 (2002) 2509–2537.
[50] L. Benabou, N.M. Abdelaziz, N. Benseddiq, Effective properties of a composite with imperfectly bonded interface, Theor. Appl. Fract. Mech. 41 (2004) 15–20.
[51] S. Nie, C. Basaran, A micromechanical model for effective elastic properties of particulate composites with imperfect interfacial bonds, Int. J. Solids Struct. 42 (2005) 4179–4191.
[52] A.L. Kalamkarov, Composite and Reinforced Elements of Construction, John Wiley & Son, Chichester, 1992.
[53] A. Bensoussan, J.L. Lions, G. Papanicolaou, Asymptotic Analysis for Periodic Structures, North-Holland, New York, 1978.
[54] E. Sanchez-Palencia, Non-Homogeneous Media and Vibration Theory, Springer Verlag, Berlin, 1980 (Lecture Notes in Physics, 127).

[55] O.A. Oleinik, G.P. Panasenko, Homogenization and asymptotic expansions for solutions of the elasticity system with rapidly oscillating periodic coefficients, Appl. Anal. 15 (1983) 15–32.
[56] N.S. Bakhvalov, G.P. Panasenko, Homogenization Averaging Processes in Periodic Media, Kluwer Academic Publishers, Dordrecht, 1989.
[57] K.D. Cherednichenko, J.A. Evans, Full two-scale asymptotic expansion and higher-order constitutive laws in the homogenization of the system of quasi-static Maxwell equation, SIAM Multiscale Model. Simul. 14 (2016) 1513–1539.
[58] H. Brito-Santana, R. Medeiros, R. Rodríguez-Ramos, V. Tita, Different interface models for calculating the effective properties in piezoelectric composite materials with imperfect fiber-matrix adhesion, Compos. Struct. 151 (2016) 70–80.
[59] I.V. Andrianov, V.I Bolshakov, V.V. Danishevs'kyy, D. Weichert, Higher order asymptotic homogenization and wave propagation in periodic composite materials, Pro. R. Soc. A 464 (2008) 1181–1201.
[60] D.W. Spring, G.H. Paulino, Computational homogenization of the debonding of particle reinforced composites: the role of interphases in interfaces, Comp. Mater. Sci. 109 (2015) 209–224.
[61] F. Lebon, S. Dumont, R. Rizzoni, J.C. López-Realpozo, R. Guinovart-Díaz, R. Rodríguez-Ramos, J. Bravo-Castillero, F.J. Sabina, Soft and hard anisotropic interface in composite materials, Compos. Part B Eng. 90 (2016) 58–68.
[62] X. Wang, P. Schiavone, A circular inhomogeneity with a mixed-type imperfect interface in anti-plane shear, Appl. Math. Model. 43 (2017) 538–547.
[63] T. Sabiston, M. Mohammadi, M. Cherkaoui, J. Levesque, K. Inal, Micromechanics for a long fibre reinforced composite model with a functionally graded interphase, Compos. Part B Eng. 84 (2016) 188–199.
[64] R. Sburlati, M. Kashtalyan, R. Cianci, Effect of graded interphase on the coefficient of thermal expansion for composites with spherical inclusions, Int. J. Solids Struct. 110–111 (2017) 80–88.
[65] J.N. Boss, V.K. Ganesh, C.T. Lim, Modulus grading versus geometrical grading of composite adherends in single-lap bonded joints, Compos. Struct. 62 (2003) 113–121.
[66] H. Brito-Santana, Y.S. Wang, R. Rodríguez-Ramos, J. Bravo-Castillero, R. Guinovart-Díaz, V. Tita, A dispersive nonlocal model for shear wave propagation in laminated composites with periodic structures, Eur. J. Mech. A Solids 49 (2015) 35–48.
[67] H. Li, L. Ying, W. Sun, Analysis of nonlinear vibration of hard coating thin plate by finite element iteration method, Shock Vib 2014 (2014) 1–12.
[68] Z. Fawaz, W. Zheng, K. Behdinan, Numerical simulation of normal and oblique ballistic impact on ceramic composite armours, Compos. Struct. 63 (2004) 387–395.